Detailed responses and a list of changes

We thank the reviewers for carefully accessing the manuscript, for the helpful comments, for the positive judgment about our study, and the specific questions and suggestions to improve the manuscript. We have carefully worked to cover each issue raised by the reviewers and revised the manuscript accordingly.

The following list of changes has been compiled such that it contains all changes to the manuscript in blue font (**new text is presented in boldface**). This should possibly remove the problem of having to cross-read two documents.

- ❑ Comments from reviewers are show in red.
- ❑ Answers to the reviews are shown in black.
- ❑ Text parts from the revised paper are shown in blue.

Associated Editor:

We received feedback from three reviewers. They all mentioned the paper is well written. However, two of them pointed out that the novelty of the manuscript is not sufficient for the RAL standard in terms of design and control. The reviewers also pointed out that a video would show more clearly its movement. The authors should better justify the new contributions of this work, and add a video. The manuscript should be revised to address all the review comments.

Our answer: We have now provided more information of design and control. We have also performed additional robot experiments (climbing on different slope angles with a soft surface (foam mat)) to justify our contribution clearly. The video of the robot climbing experiments has been also provided (http://www.manoonpong.com/Slalom/Video1.mp4). According to a reviewer's comment, we have now changed the term "flexible body" to "bendable body" in the main text and the title. The new title is "*Lateral undulation of the bendable body of a gecko-inspired robot for energy-efficient inclined surface climbing*"

Note that due to the space limitation we have now removed Fig. 1 of the previous version of the manuscript since this figure is not important and not easy to understand as pointed out by a reviewer. However, we have provided it as the front page of the supplementary video and at the git repository of the C++ code of the controller which is publicly accessible (https://bit.ly/3fXxLjH).

Review140811(Reviewer1)

This paper presents lateral undulation of the flexible body of a gecko-inspired robot for energy-efficient inclined surface climbing. To see the role of flexible body structure, the authors have compared two cases – the robot with a flexible limb and a fixed limb. By comparing the cases, the authors have proved usage of gecko's flexible limb. Therefore, the contribution of this paper is clear. In addition, the theoretical background is solid. Follows are some minor comments:

We thank the reviewer for the positive judgment about the contribution as well as the theoretical background and for your suggestion to improve the manuscript. We have addressed all the points below. We hope that the improvement makes the manuscript suitable for publication in RA-L.

1. Fig1 is not easy to understand.

Our answer: Due to the space limitation, we have now removed Fig. 1 of the previous version of the manuscript since this figure is not important and not easy to understand as pointed out by the reviewer. However, we have provided it as the front page of the supplementary video and at the git repository of the C++ code of the controller which is publicly accessible (https://bit.ly/3fXxLjH).

Basically, this figure aims to illustrate the work which includes the gecko-inspired robot and its neural control. A gecko was used as template for the robot development. Especially, we show that the robot body design is based on the bendable body of a gecko and the robot's movement is controlled by CPG-based neural control (left side). All the neurons in the figure have the same color as the complete neural circuit (Fig. 2a of the revised manuscript).

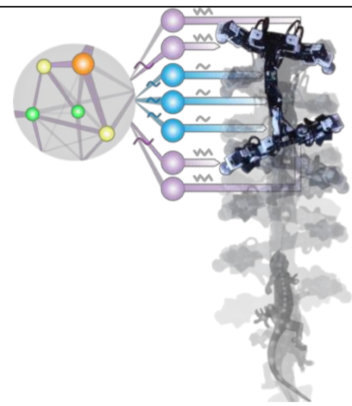

New version.

"Gecko-inspired robot (Slalom) with a bendable body for energy-efficient inclined surface climbing. The robot body design is based on an investigation of the bendable trunk and movement of Gekko gecko (bottom). A combination of lateral trunk undulation and trot gait of the robot is generated by CPG-based neural control (left)."

2. Font size in figures is too small to see.

Our answer: We have now increased the font size of all figures in the revised manuscript.

Review140817(Reviewer4)

This paper proposes a gecko-inspired robot with a flexible body with multiple active joints. The authors control the locomotion of the robot using a central pattern generator. They experimentally show that a flexible body is advantageous compared to a fixed body without active joints in term of energy efficiency with a 52% less energy consumption.

We thank the reviewer for comments and suggestions to improve the manuscript. We have now addressed all the points below. We hope that the improvement makes the manuscript suitable for publication in RA-L.

Please find comments below to help further improve the manuscript.

1. Contribution. The authors have explained the main contribution of the paper, which is about the introduction of a flexible body and its CPG-based control in a gecko-inspired robot. However, the reviewer is not convinced that the flexible body with multiple joints is novel enough considering other crawling, swimming and undulating robots with multiple active joints, which could also effectively locomote on solid surfaces.

Our answer: We have now performed new experiments and provided a comparison table to show the novelty (see below).

New experiments: Slopes with a soft[1] surface

We agreed that other crawling, swimming, and undulating robots with multiple active joints (like Salamandra robotica I, Salamandra robotica II, Pleurobot) could effectively locomote on solid surfaces. They can also swim in water/liquid. However, these robots have not shown their locomotion on a steep slope (e.g., 30 degrees) as demonstrated here. Furthermore, we have conducted new climbing experiments to demonstrate the benefit of having a bendable body with multiple joints on different slope angles with a soft surface (foam mat), such a soft slope has not been systematically tested by the other sprawling posture robots (see Table below). Our findings show that the robot with a fixed body can climb up the soft slope with a maximum angle of 20 degrees. In contrast, the robot with the bendable body can successfully climb up a steeper one with a 25-degree angle. The results have been added to new Figs. 4 and 5 of the revised manuscript (see below).

Note that due to the comment below, we have now changed the term “flexible” body to “bendable” body.

We have also provided the information of the soft slope climbing as:

[1] Soft matter can be considered between solids and liquids (https://www.global.hokudai.ac.jp/wp-content/uploads/2018/07/Soft-Matter-Material-of-the-Future.pdf).

Abstract

[…] The results in 52% **and 54%** reduced energy consumptions during climbing on steeper inclined solid **and soft surfaces, respectively,** compared to climbing with a fixed body. […]

I. INTRODUCTION

[…] i) a gecko-inspired bendable body design and movement for energy-efficient **climbing inclined solid and soft surfaces**; […]

IV. DISCUSSION AND CONCLUSION

[…] **For instance, it was unable to climb with the fixed body at a 30-degree solid slope and a 25-degree soft slope. This is because, when the angles of the solid and soft slopes were greater than 25 and 20 degrees, respectively, it began to slip on the solid slope and to get stuck on the soft slope (see http://www.manoonpong.com/Slalom/Video1.mp4).**

B. Robot climbing experiments

This climbing experiments evaluated energy efficiency while moving forward at different **solid and soft inclined surfaces with bendable and fixed-body modes**. During locomotion, the CPG-based control generated the trot gait. For the bendable body, the gait involves the body oscillation with C-shaped standing wave that is well-coordinated with the limbs. **On solid slopes, different speeds (0.10, 0.15, 0.19, 0.22, and 0.25 Hz) were investigated, whereas on soft slopes, only the most energy-efficient climbing speed (0.25 Hz) realized from solid slope climbing was investigated.**

[…] **Such control strategies were applied while climbing on soft slopes.** Snapshots of Fig. 4a **depict a 15-degree climbing by the robot on a solid inclined surface**, which corresponds to the red areas of the control signals. Photo 1 illustrates the swing phase in which the body joints reached the middle position while rotating from the right side to the left; the elevation of LF2 and RH2 was observed, while RF2 and LH2 stayed on the ground. Photo 2 shows the stance phase in which the body flexion appeared as a C-shaped standing wave on the right side while all the limbs stayed on the ground. Photo 3 shows the robot performing the opposite C-shaped body flexion during the stance phase. **Similar climbing behavior was observed on a 15-degree soft inclined surface (Fig. 4b).**

[…] It is clear that **this solid-slope climbing experiment** provide a stride frequency of 0.25 Hz, which consumed the lowest COT on each slope, and consequently it was defined as the optimal moving speed. **This frequency was employed in the soft inclined surface climbing experiment (Fig. 5). While the bendable-body robot climbed solid and soft surfaces inclined up to 30 and 25 degrees, respectively, the fixed-body robot climbed those inclined up to 25 and 20 degrees, respectively.**

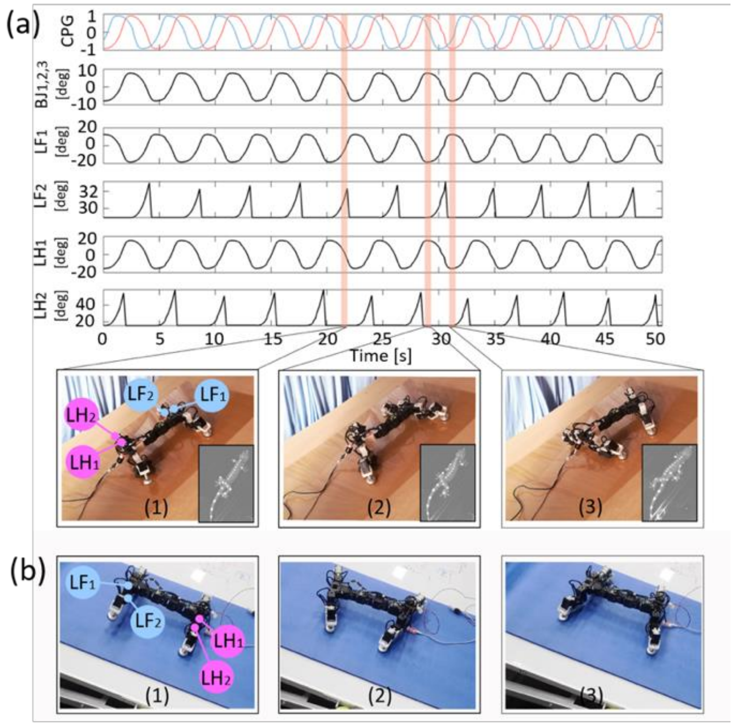

Fig. 4. Example of Slalom locomotion with the bendable body on **solid and soft inclined surfaces**. (a) The top graph shows the CPG output signals. The other graphs show the joint angles of the body (BJ1,2 ,3, see Fig. 2b), left front (LF1,2, see Fig. 2b), and left hind (LH1,2, see Fig. 2b). The snapshots below illustrate the postures of the robot and gecko during inclined solid surface climbing. **(b) The snapshots depict the robotic postures while climbing a soft inclined surface**. A video of the experiments can be seen at http://www.manoonpong.com/Slalom/Video1.mp4.

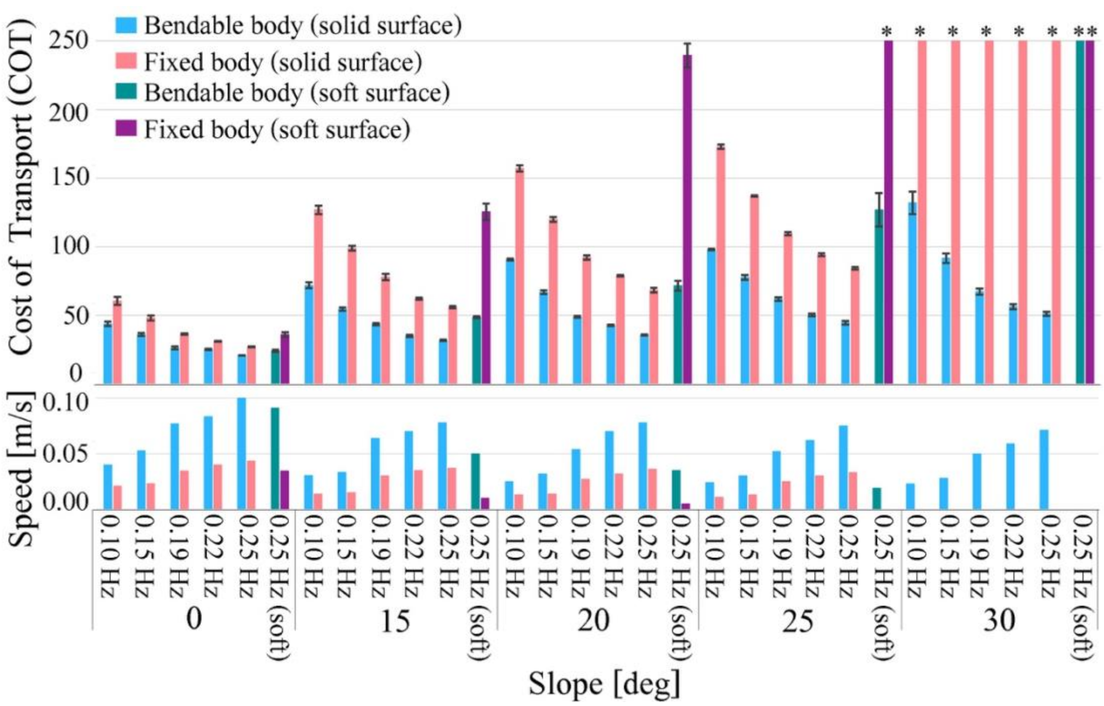

Fig. 5. **(a) COT and (b) climbing speed are being compared between movements with bendable and fixed body modes on various solid and soft slopes (0, 15, 20, 25, and 30 degree). " * " indicates the cases in which the robot failed to climb the inclined surfaces and resulted in a COT > 250.**

A comparison table: Comparing to the other state-of-the-art sprawling posture robots
To date, most existing sprawling posture robots with a bendable body (salamander-like robots (e.g., Salamandra robotica I, Salamandra robotica II, Pleurobot)) have been demonstrated for walking and swimming, while sprawling posture robots with an over-simplified fixed body (gecko-like robots (e.g., Nyxrobot, Stickybot, Gecko-inspired climbing robot, Gecko-inspired robot)) have been demonstrated for climbing. From this point of view, our robot bridges the research gap between the salamander and gecko-like robots. A comparison between our robot (Slalom) and the other state-of-the-art sprawling posture robots (Nyxrobot [15], Stickybot [17], Gecko-inspired climbing robot [16], Gecko-inspired robot [20], Salamandra robotica I [12], Salamandra robotica II [13], Pleurobot [14]) is provided as Fig. 8 in the revised manuscript as:

Robot	Control method	Multi-segmented body	Limb structure (can use adhesive material)	Locomotion modes			Surface		
				Horizontal	Slope	Vertical	Solid	Soft	Liquid
Our robot (Slalom)	CPG	✓	✓	✓	✓	✗	✓	✓	✗
Nyxrobot	IK	✗	✓	✓	✓	✗	✓	✗	✗
Stickybot	IK, Force-based controller	✗	✓	✗	✗	✓	✓	✗	✗
Gecko-inspired climbing robot	IK, Open loop controller	✗	✓	✗	✗	✓	✓	✗	✗
Gecko-inspired robot	IK, Open loop controller	✗	✓	✗	✗	✓	✓	✗	✗
Salamandra robotica I	CPGs	✓	✗	✓	✗	✗	✓	✗	✓
Salamandra robotica II	CPGs	✓	✗	✓	✗	✗	✓	✗	✓
Pleurobot	CPGs, IK	✓	✗	✓	✗	✗	✓	✗	✓

Fig. 8. A comparison between our robot (Slalom) and the other state-of-the-art sprawling posture robots (Nyxrobot [15], Stickybot [17], Gecko-inspired climbing robot [16], Gecko-inspired robot [20], Salamandra robotica I [12], Salamandra robotica II [13], Pleurobot [14]). IK: Inverse Kinematics.

Nyxrobot
D. Shao, J. Chen, A. Ji, Z. Dai, and P. Manoonpong, "Hybrid soft-rigid foot with dry adhesive material designed for a gecko-inspired climbing robot," in 2020 3rd IEEE International Conference on Soft Robotics (RoboSoft), 2020, pages 578–585.

Stickybot
S. Kim, M. Spenko, S. Trujillo, B. Heyneman, D. Santos, and M. Cutkosky, "Smooth vertical surface climbing with directional adhesion," IEEE Transactions on Robotics, volume 24, pages 65–74, 2008.

Bio-inspired climbing robot
A. Ji, Z. Zhao, P. Manoonpong, W. Wang, G. Chen, and Z. Dai, "A bio-inspired climbing robot with flexible pads and claws," Journal of Bionic Engineering, volume 15, number 2, pages 368–378, 2018.

Bio-inspired robot
Z. Wang, Z. Wang, Z. Dai, and S. Gorb, "Bio-inspired adhesive footpad for legged robot climbing under reduced gravity: Multiple toes facilitate stable attachment," Applied Sciences, volume 8, page 114, 2018.

Salamandra robotica i
A. J. Ijspeert, A. Crespi, D. Ryczko, and J.-M. Cabelguen, "From swimming to walking with a salamander robot driven by a spinal cord model," Science, volume 315, number 5817, pages 1416–1420, 2007.

Salamandra robotica ii
A. Crespi, K. Karakasiliotis, A. Guignard, and A. J. Ijspeert, "Salamandra robotica ii: An amphibious robot to study salamander-like swimming and walking gaits," IEEE Transactions on Robotics, volume 29, number 2, pages 308–320, 2013.

Pleurobot
K. Karakasiliotis, R. Thandiackal, K. Melo, T. Horvat, N. K. Mahabadi, S. Tsitkov, J. M. Cabelguen, and A. J. Ijspeert, "From cineradiography to biorobots: An approach for designing robots to emulate and study animal locomotion," Journal of The Royal Society Interface, volume 13, number 119, page 20 151 089, 2016.

2. Paper presentation and organization. The presentation and organization could be improved.
a) It is not clear to group everything in the section "Material and Methods". It is suggested that the authors organize the contents in this section into the problem formulation, experimental setup and CPG-based control.

Our answer: We have improved the revised manuscript by reorganizing Material and Methods section to the following contents. We believe that this improves the readability of the manuscript.

II Gecko-inspired design methodology
- **A. Gecko experiments and data processing**
- **B. Gecko-inspired bendable body and limb design**

III Slalom, A gecko-inspired robot
- **A. Robot hardware setup**
- **B. CPG-based neural control**

b) Explanation of Figure 7 and Figure 8 should be included in the result section rather than the discussion and conclusion section which should instead summarize the key results and discuss the limitation and future work.

Our answer: We have now moved the explanation of Figures 7 and 8 to the result section (i.e., III. EXPERIMENTAL VALIDATION OF SLALOM) and only summarized the key results and discuss the limitation and future work in the discussion and conclusion section. Note that Figures 7 and 8 have been changed to Figures 6 and 7 respectively in the revised manuscript.

III. EXPERIMENTAL VALIDATION OF SLALOM

[…] This indicates that the forelimbs make a significant effort to prevent the robot's head from moving sideways in the second half of the stance phase. Typically, a larger medio force provides higher protection of the Slalom's head tilting out in order to maintain the movement while stepping forward. **In this case, the bendable-body robot exhibited larger medio force than the fixed-body robot (see (b) in Fig. 6).**

[…] The stability is obtained because of the large medio and posterior forces, which cause the COM to oscillate laterally from side to side while a pair of diagonal supporting limbs contacts the ground intermittently in a stride. **The center of the bending moment (Fig. 7b) demonstrates the COM dynamics, which is explained by applying the lateral leg spring (LLS) model [27]. Perturbation experiments illustrated that the sprawling posture animal LLS models self-stabilized, despite control feedback [28]. The model was stable as the medio-lateral and anterior-posterior forces produced the lateral angular momentum that incurred in leg-to-leg transitions [29].**

IV. DISCUSSION AND CONCLUSION

GRF analysis demonstrated that the robot's hindlimbs generated most of the propulsion, as indicated by the posterior forces. The medio forces indicated that the forelimbs prevented the robot's head from moving sideways. The bendable-body robot exhibited greater hindlimb posterior force and forelimb medio force than the fixed-body robot. This enhanced the robot's stability while climbing steeper slopes. We calculated the bending angular momentum that resulted from the forces acting on the feet. The bendable-body robot produced a larger angular momentum, which was essential for stability during climbing. Here, the robot produced almost similar L_{AM} for all the inclined slopes where the bending radius of the bendable body was constant. In the future, we will investigate the change of bending radius to increase L_{AM} when encountering an increased slope angle, as observed in geckos [30].

3. References. The references are generally good.

Our answer: We thank the reviewer for the positive judgment about the references.

Technical concerns.

4. Why is 3-DOF design selected for the robot body? How about the design with more active joints? Do the authors expect more improvement in terms of energy efficiency when increasing the DOF of the body?

Our answer: According to our design methodology, we evaluate the number of joints that could reproduce the curvature of the gecko's body by using an error metric (see Fig. 1c in the revised manuscript). Although the more joints, the better the ability to capture the bending shapes of the gecko's body during locomotion, the exponential of the total error value begins to converge to our acceptable point (i.e., 5% total error) at three DOFs. As a result, we chose three-body joints as the bare minimum of joints required for the robot to imitate the gecko's body posture, as well as a reasonable trade-off based on the geometry and resulting length and weight of the robot.

The length and weight of the robot with three body joints are 35cm and 2.45kg, respectively. If we design with more active joints such as six body joints, the error matric (Fig. 1c) shows a good geometry with approximately 2% total error. However, robot locomotion efficiency depends not only on the geometry but also on the weight and size. With the six joints, the robot length will be 52.5cm and its weight will be 3kg. This will lead to 22% heavier and can affect the locomotion performance by typically consuming more energy. Thus increasing the DOF of the body might not improve the robot's energy efficiency but will make the robot heavier which will be difficult to climb up a steep slope or a wall in the future.

We have now provided estimated weights at different DOFs in Fig. 1.

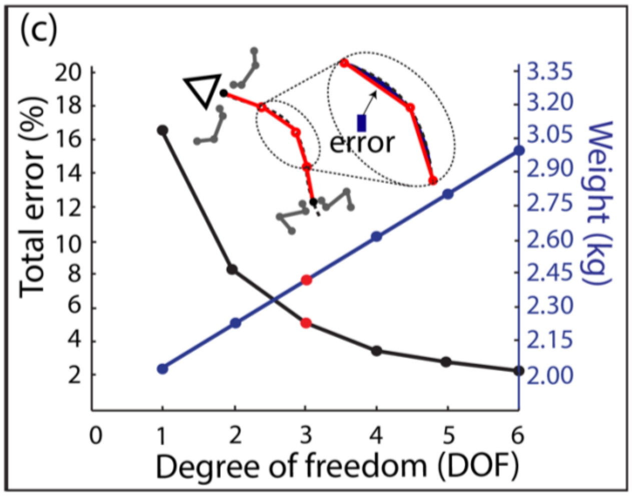

Fig. 1: […] (c) An error area between the observed trunk bending in the Gecko and the segmented line with different joint numbers were considered. The resulting number of joints (three, indicated by red point) was selected as a trade-off between the accuracy of the approximation and the minimal number of joints. **Robot weight was estimated as a function of the DOFs. The robot weight was 7%, 14%, or 22% heavier than the three DOFs, when four, five, or six DOFs were selected, respectively. Likewise, the power consumption increased to 10%, 21%, 32%.** (d) […]

5. "Flexible" is a little misleading here. Is there any impedance or elastic property encoded in the active joint like a soft-body in the real gecko?

Our answer: We have now replaced the term "flexible" to "bendable" to avoid confusion since in this work we have not included any impedance or elastic property encoded in the active joints. However, we are currently investigating on implementing adaptive muscle models for the flexible/elastic property, like a soft-body in the real gecko. This information has been provided in the revised manuscript as:

[…] This extension will allow the robot to efficiently achieve different locomotion modes, such as walking, swimming, and climbing (up and down on inclined surfaces and walls). We will apply adaptive muscle models [32] to encode an elastic property resembling a real gecko-like flexible body.

[32] C. V. Huerta, X. Xiong, P. Billeschou, and P. Manoonpong, "Adaptive neuromechanical control for robust behaviors of bio-inspired walking robots," in Neural Information Processing, Cham: Springer International Publishing, 2020, pages 775–786.

6. A dynamic model of the robot will be beneficial to help understand and explain the energy efficiency improvement of the flexible robot body compared with a rigid robot body. However, such a dynamic model is not available currently in this paper.

Our answer: Robot energy efficiency is influenced by a number of factors. One of them is the length of a robot's stride, which shows a clear distinction between fixed and bendable body configurations. Thus, we focus on analyzing a stride length involved in energy efficiency using a simplified geometrical model [26] (see Fig. LOC1). In this model, we assume that stride lengths are constant, and the movements of the left and right legs are symmetrical. We can calculate the stride length of both body configurations based on the assumption:

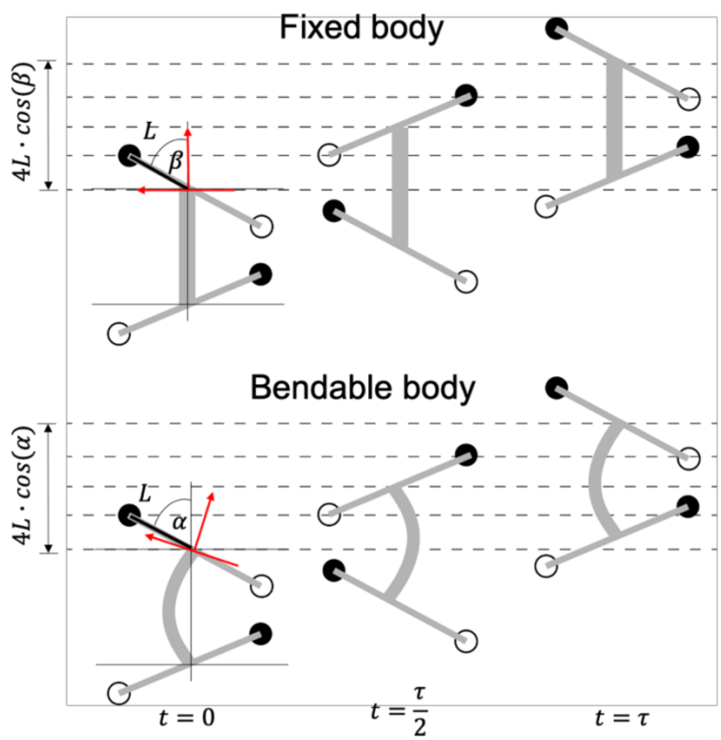

Fig_LOC1: A stride length of the robot with the fixed (top) and bendable bodies (bottom), where τ is a stride length.

$$D_{fixed} = 4L \cdot cos(\beta), \quad (1)$$
$$D_{bend} = 4L \cdot cos(\alpha), \quad (2)$$

where D_{fixed} and D_{bend} are a stride length of the fixed and bendable bodies, respectively, and L is the leg length (i.e., 17.3 cm) which is set to a constant value during a stance phase.

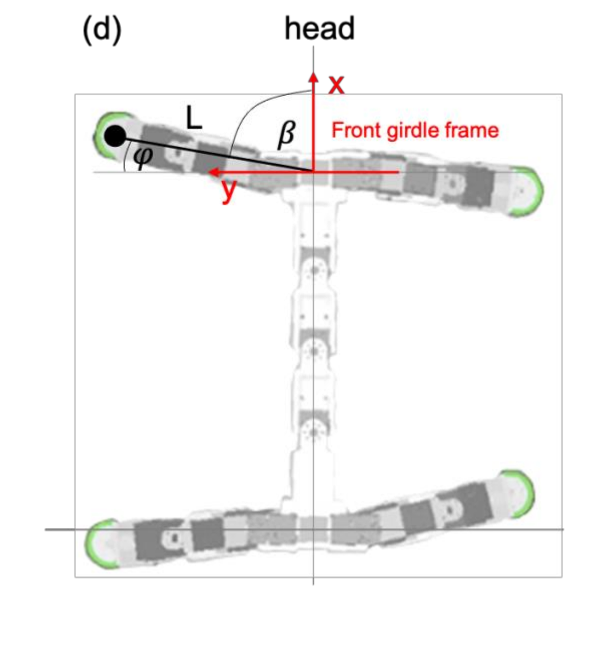

Fig_LOC2: A geometrical model of the fixed body.

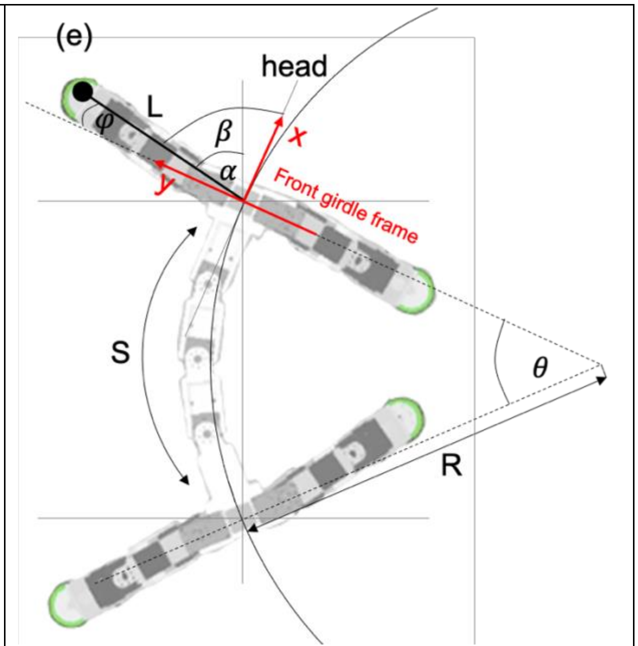

Fig_LOC3: A geometrical model of the bendable body.

Based on the geometrical model in Fig. LOC2 and Fig. LOC 3, we rewrite equations (1) and (2) in terms of the representative variables (φ, R) to illustrate the robot postures. φ is the angle between the foot location and the y-axis of the girdle frame at the beginning of each stride, and R is the bending radius of the bendable body. From the geometric relationship of the model, we obtain the following question:

$$\beta = 90 - \varphi, \tag{3}$$

$$\alpha = 90 - \varphi - \frac{\theta}{2}, \tag{4}$$

using the segment of a circle formula ($S = \frac{\theta}{180}\pi R$), where θ unit is degree. Thus, we can express the equation (4) by substituting θ as:

$$\alpha = 90 - \varphi - \frac{90}{\pi} \cdot \frac{S}{R}, \tag{5}$$

substituting β (equation (3)) and α (equation (5)) to the equations (1) and (2), respectively, we obtain general equations with the two variables as follows:

$$D_{fixed} = 4L \cdot cos(90 - \varphi), \tag{6}$$

$$D_{bend} = 4L \cdot cos(90 - \varphi - (\frac{90}{\pi} \cdot \frac{S}{R})), \tag{7}$$

where S is the body length (i.e., 35 cm).

From our neural control, the motor signals generate a trot gait where φ is 17 degrees for both configurations and R is 41.7 cm for the bendable body. Based on the model, the stride lengths of the fixed body (D_{fixed}) and bendable body (D_{bend}) are 20.2 cm and 45.3 cm, respectively. According to this, the stride length of the bendable body is approximately 2.24 times larger than that of the fixed body ($D_{bend} \sim 2.24 D_{fixed}$).

We assume that the bendable-body robot and fixed-body robot have the same mass (m) and almost the same energy usage (E). Based on the assumption and geomatical analysis, the COT ratio can be described as follows:

$$\frac{\mathrm{COT}_{bend}}{\mathrm{COT}_{fixed}} = \frac{\frac{E_{bend}}{mgD_{bend}}}{\frac{E_{fixed}}{mgD_{fixed}}} = \frac{\frac{E_{bend}}{2.24D_{fixed}}}{\frac{E_{fixed}}{D_{fixed}}} \cong 0.45,$$

$$\therefore \quad \mathrm{COT}_{bend} \cong 0.45\mathrm{COT}_{fixed}.$$

To sum up, our analysis shows that the COT of the bendable body is reduced approximately 55% when compared with the fixed body.

Finally, the climbing experiments (Fig.5) show that the robot with the bendable body can improve energy efficiency where the COT of the bendable body was approximately 52% (54%) lower than that of the fixed body for all solid (soft) slopes ($\mathrm{COT}_{bend} \sim 0.48\mathrm{COT}_{fixed}$ for solid slopes, $\mathrm{COT}_{bend} \sim 0.46\mathrm{COT}_{fixed}$ for soft slopes.

Due to the space limitation, we have now minimally provided this information in Fig. 2d and e.

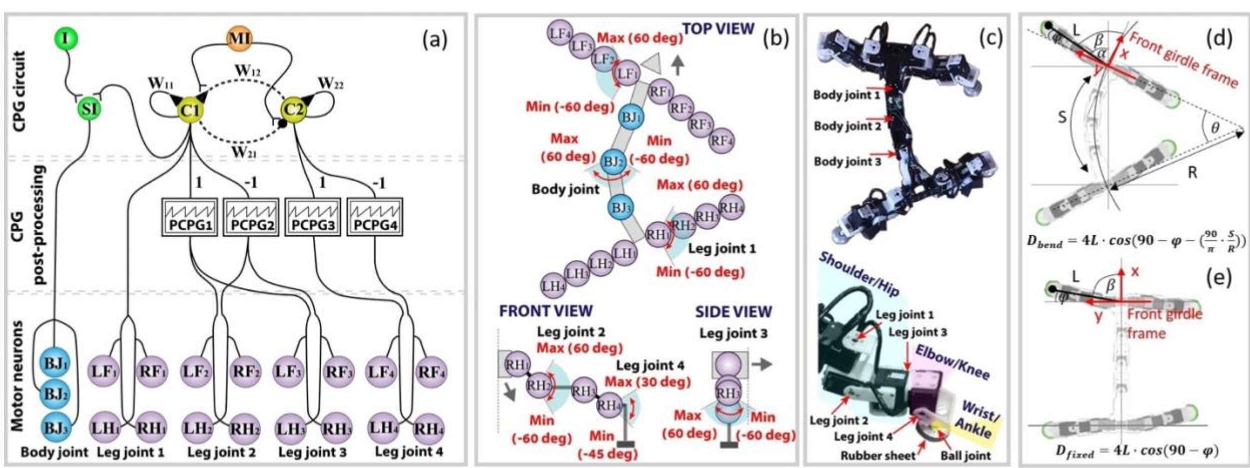

Fig. 2. Architecture of the simplified CPG-based controller. (a) Neural circuit for controlling the gecko-inspired robot. (b) Location of the motor neurons on the robot and their movements.

Minimum and maximum angles of the body joints, leg joint 1, leg joint 2, leg joint 3 and leg joint 4. (c) Example of components at the body joints and the left hind leg (LH). **(d), (e) Geometrical models of the bendable and fixed bodies. The models can be used to analyze the energy efficiency improvement based on a stride length of the bendable robot body (D_{bend}) compared with the fixed robot body (D_{fixed}). φ is the angle between the foot location and the y-axis of the girdle frame at the beginning of each stride (i.e., 17 degrees). R is the bending radius of the bendable body (i.e., 41.7 cm). L is the leg length (i.e., 17.3 cm). S is the body length (i.e., 35 cm). According to the parameter values obtained from the real robot movements driven by the neural control, D_{bend} is proximately 2.24 times larger than D_{fixed}. The bendable-body robot treaded longer than the fixed-body robot during each stride. Therefore, the cost of transport (COT) of the bendable-body robot was lower than that of the fixed-body robot ($COT_{bend} \cong \frac{COT_{fixed}}{2.24}$, assuming that both robot configurations have the same mass (m) and almost the same energy usage (E)). The COT formula is shown in section IV. D_{bend} and D_{fixed} derivation formulae can be accessed at https://bit.ly/3fXxLjH. Our robot climbing experimental observations (Fig. 5) followed COT estimations.**

[26] K. Mombaur, H. Vallery, Y. Hu, J. Buchli, P. Bhounsule, T. Boaventura,P. M. Wensing, S. Revzen, A. D. Ames, I. Poulakakis, and A. Ijspeert, "Chapter 4 - control of motion and compliance," in Bioinspired Legged Locomotion, M. A. Sharbafi and A. Seyfarth, Eds., Butterworth-Heinemann, 2017, pages 135–346.

7. The metric Cost of Transportation (COT) has been used and compared between the flexible and fixed robot body designs in this paper. How about the whole-body moving speeds? Currently, there is no quantitative comparison of speed in the manuscript.

Our answer: We have now added the whole-body climbing speeds in Fig. 5.

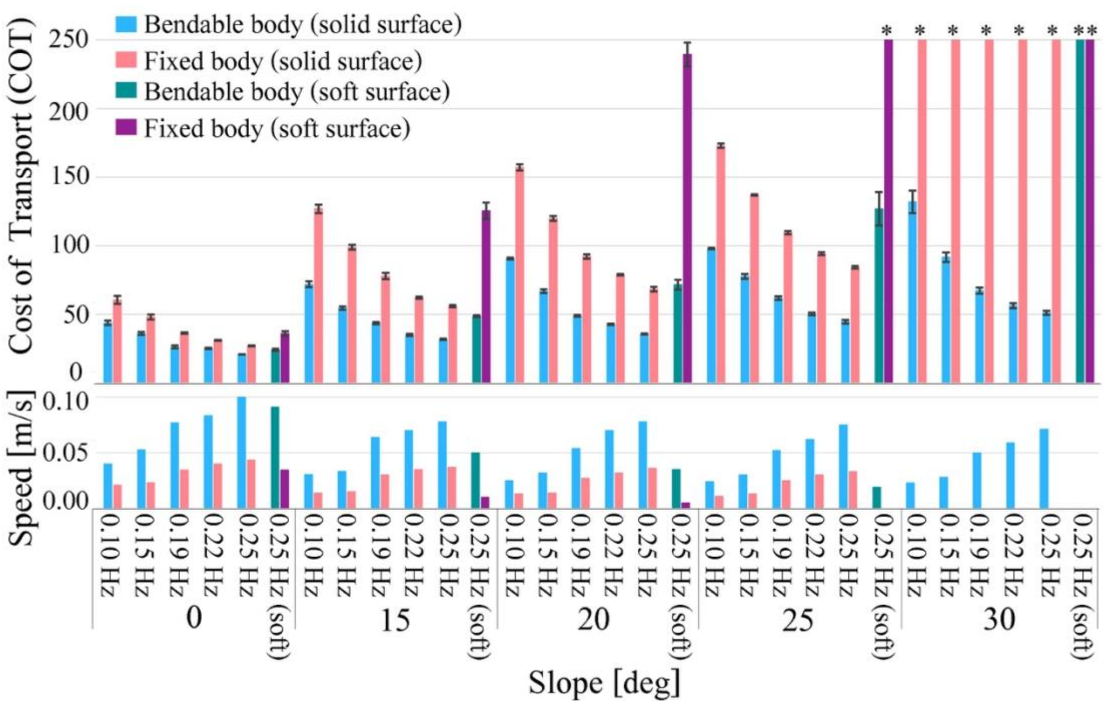

Fig. 5. **(a) COT and (b) climbing speed are being compared between movements with bendable and fixed body modes on various solid and soft slopes (0, 15, 20, 25, and 30 degree). " * " indicates the cases in which the robot failed to climb the inclined surfaces and resulted in a COT > 250.**

8. In Figure 8c, it is not clear whether the difference in the bending angular momentums of the two designs is significant or not. The authors need to explain and justify why they choose this metric and why the difference is significant to justify the usefulness of their flexible design.

Our answer: Figure 8c has been now changed to Figure 7c in the revised manuscript. To date, many researchers have studied the stability of sprawling posture animals and found that the lateral ground reaction forces is an essential key to define its stability locomotion. Kubow and Full (1999) created a first dynamic model of a six-legged anchored for defining stability and maneuverability in sprawling posture animals. The movement of the model was controlled by providing the medio-lateral and anterior-posterior forces, which were measured in cockroaches. Surprisingly, the model could passively self-stabilized to perturbation without the aid of control feedback [28].

In addition, Schmitt and Holmes (2000a, b) represented the synergistic behavior of the insect's leg by applying the lateral leg spring (LLS) model. The LLS model consists of a single leg spring connected to the center of pressure (P) on the body (Fig._LOC3). Perturbation experiments illustrated that the model self-stabilizes as it walks forward with laterally oscillating side to side. The model obtained stability because the medio-lateral and anterior-posterior forces produce the lateral angular momentum incurred in leg-to-leg transitions [29].

Based on previous studies, we found that they have a strongly reasonable explanation of stability with respect to the lateral angular momentums. This is the reason why we choose the bending angular momentum to evaluate stability in our study.

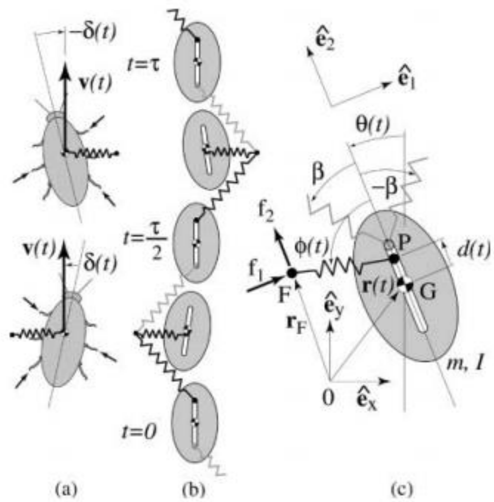

Fig._LOC3: (a) Overhead views of a cockroach. (b) A cartoon of the LLS model during a stride. (c) Model details from [29].

Moreover, GRFs of geckos moving on different slopes are used to reveal how the lateral bending of the body responds to changing slope [30]. The observations show that the minimum bending radius continually decreases with an increase in the slope, indicating that geckos bend their spine to increase the bending angular momentum (L_{AM}) when the slope increase (Fig._LOC4). It is evident that the gain of bending angular momentum is meaningful for maintaining stability in sprawling posture animals when climbing on a slope. This is also the reason why the difference L_{AM} is significant to justify the usefulness of body bending for climbing.

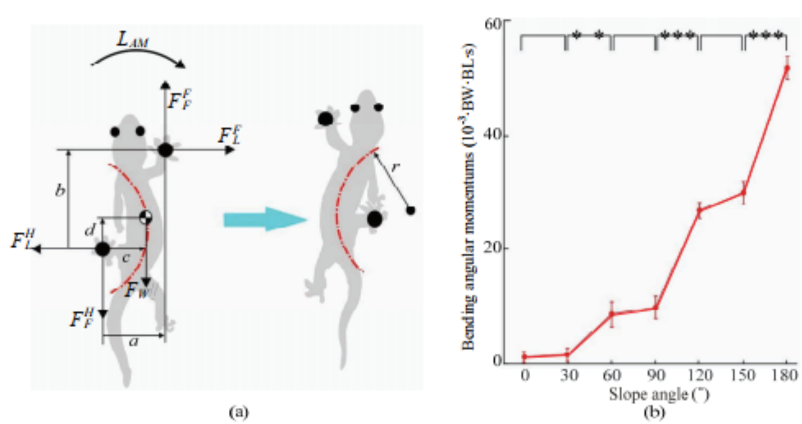

Fig._LOC4: (a) Diagram of the calculation for bending angular momentum. (b) Mean values of the bending angular momentum of geckos climbing on different slopes from [30].

In "C. Ground reaction force analysis", we have provided this information as:

[…] The center of the bending moment (Fig. 7b) demonstrates the COM dynamics, which is explained by applying the lateral leg spring (LLS) model **[27]. Perturbation experiments illustrated that the sprawling posture animal LLS models self-stabilized, despite control feedback [28]. The model was stable as the medio-lateral and anterior-posterior forces produced the lateral angular momentum that incurred in leg-to-leg transitions [29].**

[28] T. M. Kubow, "The role of the mechanical system in control: A hypothesis of self-stabilization in hexapedal runners," Philosophical Transactions of the Royal Society B: Biological Sciences, volume 354, number 1385, pages 849–861, May 1999.

[29] J. Schmitt, M. Garcia, R. C. Razo, P. Holmes, and R. J. Full, "Dy- namics and stability of legged locomotion in the horizontal plane: A test case using insects," Biological Cybernetics, volume 86, number 5, pages 343–353, 2002.

Schmitt, J. and Holmes, P. (2000a). Mechanical models for insect locomotion: Dynamics and stability in the horizontal plane. I. Theory. Biol. Cybern. 83, 501-515.

Schmitt, J. and Holmes, P. (2000b). Mechanical models for insect locomotion: Dynamics and stability in the horizontal plane. II. Application. Biol. Cybern. 83, 517-527.

Other concerns.

9. The last column at slope angle 30 in Figure 6 seems truncated.

Our answer: Noted that Figure 6 has been changed to Figure 5 in the revised manuscript. The last column of Figure 5 is the COT compared between the robot movements with the bendable and fixed body when the robot climbed up on the 30-degree slope with various stride frequencies (0.10, 0.15, 0.19, 0.22, and 0.25 Hz). We let the robot climb 10 trials and record the experimental data when the robot successfully 100% traversed to 1m distance without falling and human intervention. However, the robot could not climb with a fixed body (i.e., without lateral body movement) on the 30-degree slope for all frequencies. The success rate is 0% because the robot always slipped and stayed at the starting point. This leads to the COT values of the fixed body (more than 250). To make it more clear, we have now added " * " on top of the graph to indicate the robot failed to walk up the slope.

We have added more explanation in the revised captions of Figure 5:

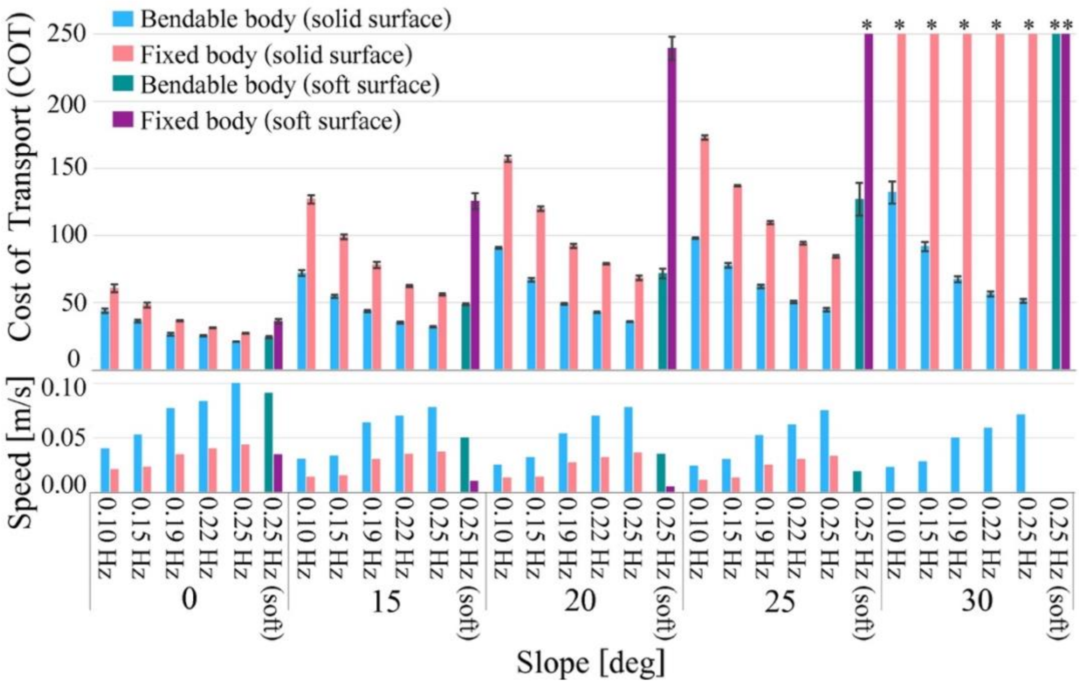

Fig. 5. **(a) COT and (b) climbing speed are being compared between movements with bendable and fixed body modes on various solid and soft slopes (0, 15, 20, 25, and 30 degree). " * " indicates the cases in which the robot failed to climb the inclined surfaces and resulted in a COT > 250.**

10. In Figure 7, a-f should be explained in the captions.

Our answer: Noted that Figure 7 has been changed to Figure 6 in the revised manuscript. We have now added the explanation of a-f in the revised captions of Figure 6:

"Fig.6. Comparison of ground reaction forces (GRFs) in fixed and bendable body movements. Left forelimb and left hindlimb GRFs were measured and analyzed with respect to medio-lateral (Fx), anterior-posterior (Fy) and normal (Fz). **The robot with a bendable body produces medio-lateral forces in the forelimb, including (a) lateral peak force, (b) medio peak force, and (c) lateral force during slip. For the anterior-posterior forces, the forelimb always produces a posterior force below 4N (d) while the force reaches 6N (e) for the hindlimb. The normal forces of both the bendable and fixed bodies are similar (f).** Each snapshot below shows the body postures and the position of feet on/off the ground during climbing."

11. The paper does not have a multimedia attachment. However, it is highly suggested that a video should be included to show the experimental results and comparisons.

Our answer: We have now provided a supplementary video and mentioned it in the revised manuscript as:

Fig. 4: […] A video of the experiments can be seen at http://www.manoonpong.com/Slalom/Video1.mp4.

Review150327(Reviewer6)

The paper presents the design of a gecko robot and its control. The claim of the paper is the distribution of joints in the sprawlings shape of the robot allowing this having an optimal flexibility for better climbing (reduction of 52% if energy consumption compared to fixed body robot). The control is based on central pattern generator (CPG) based neural network. Finally , experiments are carried out.

The paper is well written. However, I have the following concerns.

We thank the reviewer for the positive judgment and for your comments and suggestions to improve the manuscript. We have now addressed all point below. We hope that the improvement makes the manuscript suitable for publication in RA-L.

The claimed contribution in term of design is clarified in the paper. Meanwhile, from the literature, its novelty seems to be not justified.

Our answer: We have now performed new experiments and provided a comparison table to show the novelty (see below).

New experiments: Slopes with a soft[2] surface
We agreed that other crawling, swimming, and undulating robots with multiple active joints (like Salamandra robotica I, Salamandra robotica II, Pleurobot) could effectively locomote on solid surfaces. They can also swim in water/liquid. However, these robots have not shown their locomotion on a steep slope (e.g., 30 degrees) as demonstrated here. Furthermore, we have conducted new climbing experiments to demonstrate the benefit of having a bendable body with multiple joints on different slope angles with a soft surface (foam mat), such a soft slope has not been systematically tested by the other sprawling posture robots (see Table below). Our findings show that the robot with a fixed body can climb up the soft slope with a maximum angle of 20 degrees. In contrast, the robot with the bendable body can successfully climb up a steeper one with a 25-degree angle. The results have been added to new Figs. 4 and 5 of the revised manuscript (see below).

Note that due to the comment below, we have now changed the term “flexible” body to “bendable” body.

We have also provided the information of the soft slope climbing as:

Abstract

[…] The results in 52% **and 54%** reduced energy consumptions during climbing on steeper inclined solid **and soft surfaces, respectively,** compared to climbing with a fixed body. […]

---

[2] Soft matter can be considered between solids and liquids (https://www.global.hokudai.ac.jp/wp-content/uploads/2018/07/Soft-Matter-Material-of-the-Future.pdf).

I. INTRODUCTION

[…] i) a gecko-inspired bendable body design and movement for energy-efficient **climbing inclined solid and soft surfaces**; […]

IV. DISCUSSION AND CONCLUSION

[…] **For instance, it was unable to climb with the fixed body at a 30-degree solid slope and a 25-degree soft slope. This is because, when the angles of the solid and soft slopes were greater than 25 and 20 degrees, respectively, it began to slip on the solid slope and to get stuck on the soft slope (see http://www.manoonpong.com/Slalom/Video1.mp4).**

B. Robot climbing experiments

This climbing experiments evaluated energy efficiency while moving forward at different **solid and soft inclined surfaces with bendable and fixed-body modes**. During locomotion, the CPG-based control generated the trot gait. For the bendable body, the gait involves the body oscillation with C-shaped standing wave that is well-coordinated with the limbs. **On solid slopes, different speeds (0.10, 0.15, 0.19, 0.22, and 0.25 Hz) were investigated, whereas on soft slopes, only the most energy-efficient climbing speed (0.25 Hz) realized from solid slope climbing was investigated.**

[…] **Such control strategies were applied while climbing on soft slopes.** Snapshots of Fig. 4(a) **depict a 15-degree climbing by the robot on a solid inclined surface**, which corresponds to the red areas of the control signals. Photo 1 illustrates the swing phase in which the body joints reached the middle position while rotating from the right side to the left; the elevation of LF2 and RH2 was observed, while RF2 and LH2 stayed on the ground. Photo 2 shows the stance phase in which the body flexion appeared as a C-shaped standing wave on the right side while all the limbs stayed on the ground. Photo 3 shows the robot performing the opposite C-shaped body flexion during the stance phase. **Similar climbing behavior was observed on a 15-degree soft inclined surface (Fig. 4b).**

[…] It is clear that **this solid-slope climbing experiment** provide a stride frequency of 0.25 Hz, which consumed the lowest COT on each slope, and consequently it was defined as the optimal moving speed. **This frequency was employed in the soft inclined surface climbing experiment (Fig. 5). While the bendable-body robot climbed solid and soft surfaces inclined up to 30 and 25 degrees, respectively, the fixed-body robot climbed those inclined up to 25 and 20 degrees, respectively.**

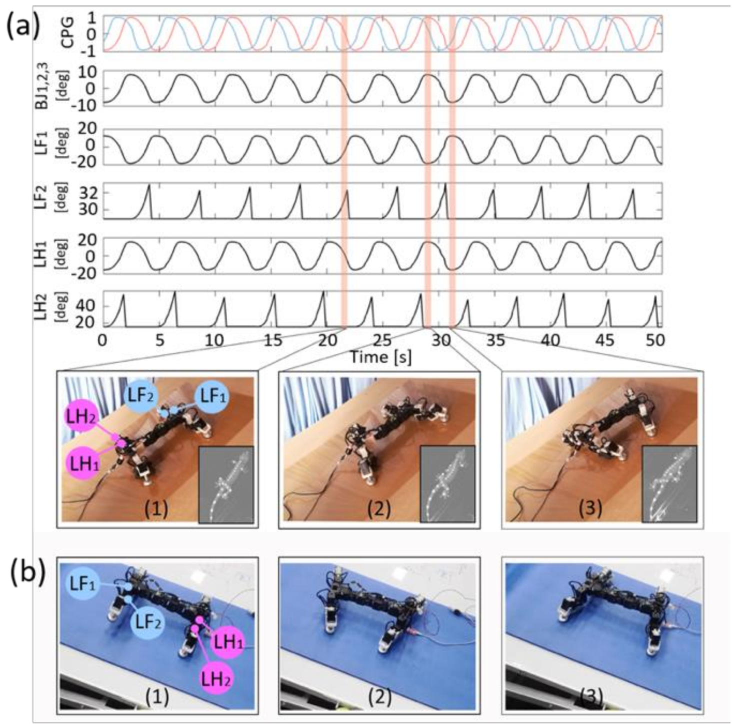

Fig. 4. Example of Slalom locomotion with the bendable body on **solid and soft inclined surfaces**. (a) The top graph shows the CPG output signals. The other graphs show the joint angles of the body (BJ1,2 ,3, see Fig. 2b), left front (LF1,2, see Fig. 2b), and left hind (LH1,2, see Fig. 2b). The snapshots below illustrate the postures of the robot and gecko during inclined solid surface climbing. **(b) The snapshots depict the robotic postures while climbing a soft inclined surface**. A video of the experiments can be seen at http://www.manoonpong.com/Slalom/Video1.mp4.

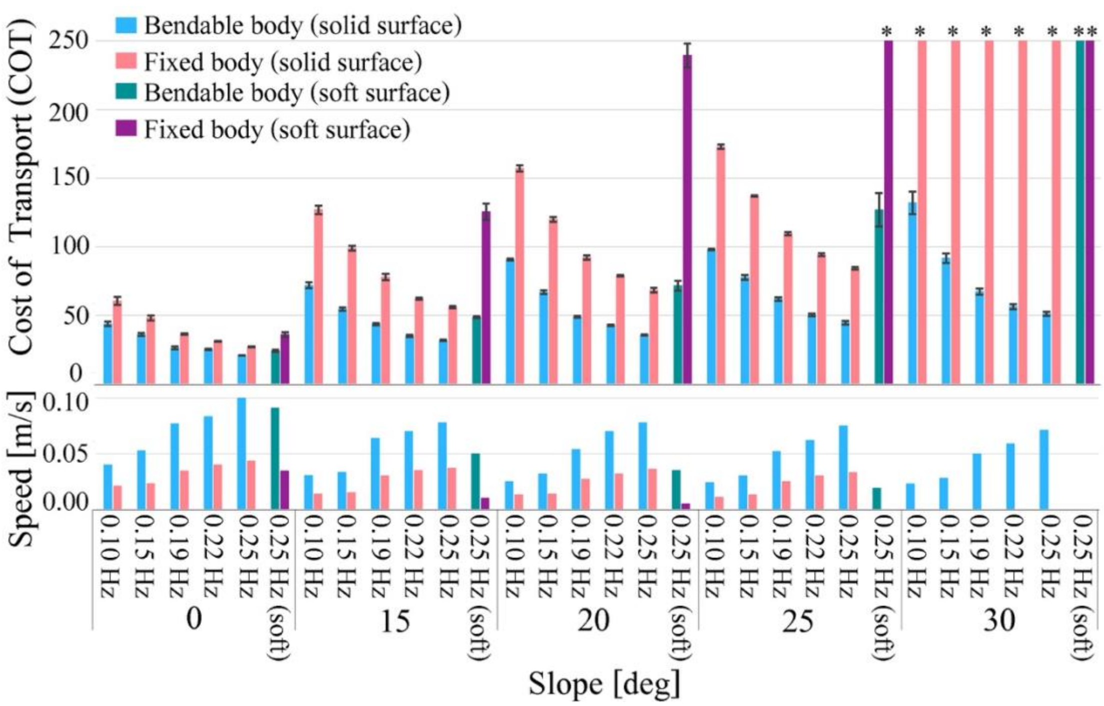

Fig. 5. **(a) COT and (b) climbing speed are being compared between movements with bendable and fixed body modes on various solid and soft slopes (0, 15, 20, 25, and 30 degree). " * " indicates the cases in which the robot failed to climb the inclined surfaces and resulted in a COT > 250.**

A comparison table: Comparing to the other state-of-the-art sprawling posture robots

To date, most existing sprawling posture robots with a bendable body (salamander-like robots (e.g., Salamandra robotica I, Salamandra robotica II, Pleurobot)) have been demonstrated for walking and swimming, while sprawling posture robots with an over-simplified fixed body (gecko-like robots (e.g., Nyxrobot, Stickybot, Gecko-inspired climbing robot, Gecko-inspired robot)) have been demonstrated for climbing. From this point of view, our robot bridges the research gap between the salamander and gecko-like robots. A comparison between our robot (Slalom) and the other state-of-the-art sprawling posture robots (Nyxrobot [15], Stickybot [17], Gecko-inspired climbing robot [16], Gecko-inspired robot [20], Salamandra robotica I [12], Salamandra robotica II [13], Pleurobot [14]) is provided as Fig. 8 in the revised manuscript as:

Robot	Control method	Multi-segmented body	Limb structure (can use adhesive material)	Locomotion modes			Surface		
				Horizontal	Slope	Vertical	Solid	Soft	Liquid
Our robot (Slalom)	CPG	✓	✓	✓	✓	✗	✓	✓	✗
Nyxrobot	IK	✗	✓	✓	✓	✗	✓	✗	✗
Stickybot	IK, Force-based controller	✗	✓	✗	✗	✓	✓	✗	✗
Gecko-inspired climbing robot	IK, Open loop controller	✗	✓	✗	✗	✓	✓	✗	✗
Gecko-inspired robot	IK, Open loop controller	✗	✓	✗	✗	✓	✓	✗	✗
Salamandra robotica I	CPGs	✓	✗	✓	✗	✗	✓	✗	✓
Salamandra robotica II	CPGs	✓	✗	✓	✗	✗	✓	✗	✓
Pleurobot	CPGs, IK	✓	✗	✓	✗	✗	✓	✗	✓

Fig. 8. A comparison between our robot (Slalom) and the other state-of-the-art sprawling posture robots (Nyxrobot [15], Stickybot [17], Gecko-inspired climbing robot [16], Gecko-inspired robot [20], Salamandra robotica I [12], Salamandra robotica II [13], Pleurobot [14]). IK: Inverse Kinematics.

Nyxrobot

D. Shao, J. Chen, A. Ji, Z. Dai, and P. Manoonpong, "Hybrid soft-rigid foot with dry adhesive material designed for a gecko-inspired climbing robot," in 2020 3rd IEEE International Conference on Soft Robotics (RoboSoft), 2020, pages 578–585.

Stickybot

S. Kim, M. Spenko, S. Trujillo, B. Heyneman, D. Santos, and M. Cutkosky, "Smooth vertical surface climbing with directional adhesion," IEEE Transactions on Robotics, volume 24, pages 65–74, 2008.

Bio-inspired climbing robot

A. Ji, Z. Zhao, P. Manoonpong, W. Wang, G. Chen, and Z. Dai, "A bio-inspired climbing robot with flexible pads and claws," Journal of Bionic Engineering, volume 15, number 2, pages 368–378, 2018.

Bio-inspired robot
Z. Wang, Z. Wang, Z. Dai, and S. Gorb, "Bio-inspired adhesive footpad for legged robot climbing under reduced gravity: Multiple toes facilitate stable attachment," Applied Sciences, volume 8, page 114, 2018.

Salamandra robotica i
A. J. Ijspeert, A. Crespi, D. Ryczko, and J.-M. Cabelguen, "From swimming to walking with a salamander robot driven by a spinal cord model," Science, volume 315, number 5817, pages 1416–1420, 2007.

Salamandra robotica ii
A. Crespi, K. Karakasiliotis, A. Guignard, and A. J. Ijspeert, "Salamandra robotica ii: An amphibious robot to study salamander-like swimming and walking gaits," IEEE Transactions on Robotics, volume 29, number 2, pages 308–320, 2013.

Pleurobot
K. Karakasiliotis, R. Thandiackal, K. Melo, T. Horvat, N. K. Mahabadi, S. Tsitkov, J. M. Cabelguen, and A. J. Ijspeert, "From cineradiography to biorobots: An approach for designing robots to emulate and study animal locomotion," Journal of The Royal Society Interface, volume 13, number 119, page 20 151 089, 2016.

The design and the functioning of the robot are hard to see without video. It is not fair to present moving robot with different photos and curves (which are not finally really representative) while video could have accompanied the paper.

Our answer: We have now provided a supplementary video and mentioned it in the revised manuscript as:

Fig. 4: […] A video of the experiments can be seen at http://www.manoonpong.com/Slalom/Video1.mp4.

The control law is based on previous work (see [24]) which apparently was more general. The real contribution in term of control here is therefore questionable.

Our answer: When designing a controller for a sprawling posture robot with an active bendable/flexible body, the coordination between the body and legs is important. Most of these robots uses inverse kinematics requiring a robot kinematic model and/or complex multiple CPGs requiring a CPG synchronization mechanism (e.g., Pleurobot, Salamandra robotica I-II) to generate C-shaped standing and/or S-shaped traveling waves for their body movement. For example, Pleurobot is driven by multiple CPGs to coordinate between legs and body with a standing wave for walking on the ground or generate a traveling body patten for swimming in the water.

So far, a single oscillator (a CPG) has not been fully explored for controlling a sprawling posture robot with an active bendable/flexible body, especially generating both various gaits and traveling body patterns. Our research question is *"Is it possible to coordinate legs with lateral undulation patterns of the body using only one single oscillator?"* Achieving this will reduce control complexity of a sprawling posture robot with an active bendable/flexible body and will also create a follow-up question *"why do animals have multiple CPGs?"*

From this point of view, we aim to use CPG-based neural control with a single CPG to well-coordinated legs with various body patterns for achieving versatile locomotor behaviors including walking, swimming, and climbing. And we would like to see the limit of the simplified control approach to gain a better understand of animal locomotion control.

In this paper, our contribution in terms of control is that a single CPG can control the bendable body and leg coordination to achieve a trot gait and lateral body undulation with a C-shaped standing wave (Fig._LOC1, left). The simplified CPG-based neural control does not require a robot kinematic model or complex synchronization mechanism between CPGs. Recently, we have realized that it is possible to generate both standing and traveling waveforms of lateral body movement by simply adding delay lines (t) and to generate proper leg trajectory for climbing/walking with various traveling body waveforms by applying a fast learning/trajectory optimization method [Thor et al., 2020] (Fig._LOC1, right).

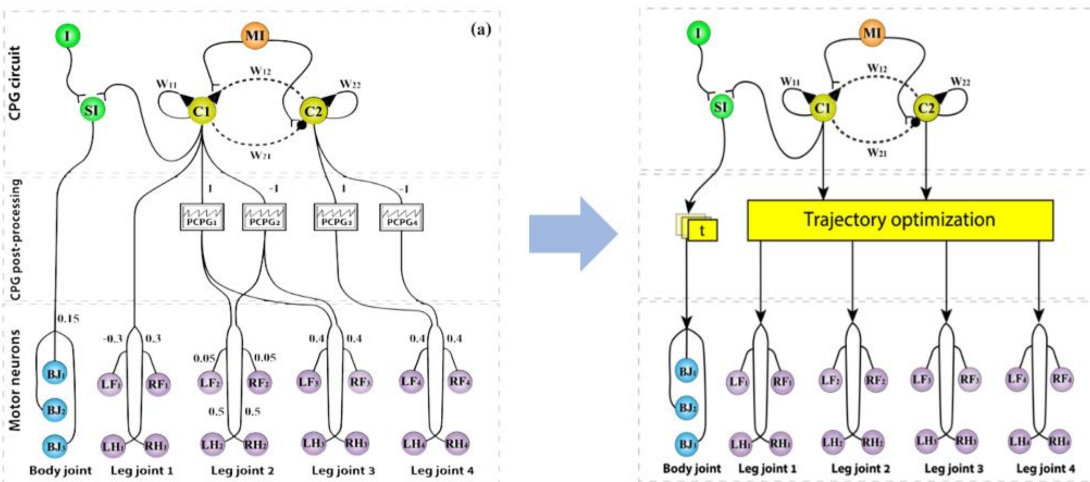

Fig._LOC1: Left, Neural control with a single CPG (shown in this study). Right, its extension for generating various traveling waveforms with proper leg movements.

In the future, the control framework will be extended with delay lines and leg trajectory optimization (as shown in Fig._LOC1, right). The trajectory optimization can be achieved by using premotor neural networks (e.g., radial basis networks) with a learning mechanism (e.g., PI^{BB}) for learning optimal coordination of leg and body patterns of standing and traveling waves (Fig._LOC2).

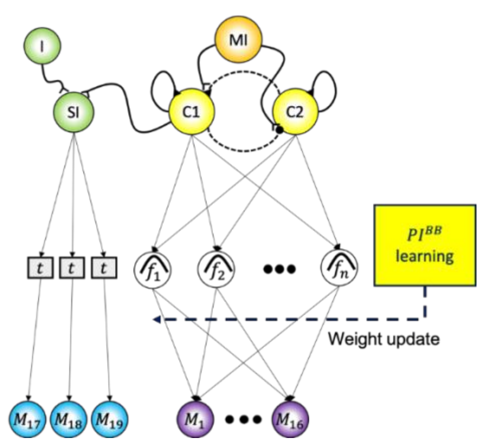

Fig._LOC2: The extended neural CPG-based control with delay lines, RBFNs, and PI^{BB} for versatile locomotion behaviors.

A preliminary result of this extended control for walking with both standing and traveling waves can be seen at www.manoonpong.com/Slalom/Video2.mp4. However, presenting this in the manuscript will go beyond the scope of this work.

To clarify our control contribution, we have now provided a comparison table:

Robot	Control method	Multi-segmented body	Limb structure (can use adhesive material)	Locomotion modes			Surface		
				Horizontal	Slope	Vertical	Solid	Soft	Liquid
Our robot (Slalom)	CPG	✓	✓	✓	✓	✗	✓	✓	✗
Nyxrobot	IK	✗	✓	✓	✓	✗	✓	✗	✗
Stickybot	IK, Force-based controller	✗	✓	✗	✗	✓	✓	✗	✗
Gecko-inspired climbing robot	IK, Open loop controller	✗	✓	✗	✗	✓	✓	✗	✗
Gecko-inspired robot	IK, Open loop controller	✗	✓	✗	✗	✓	✓	✗	✗
Salamandra robotica I	CPGs	✓	✗	✓	✗	✗	✓	✗	✓
Salamandra robotica II	CPGs	✓	✗	✓	✗	✗	✓	✗	✓
Pleurobot	CPGs, IK	✓	✗	✓	✗	✗	✓	✗	✓

Fig. 8. A comparison between our robot (Slalom) and the other state-of-the-art sprawling posture robots (Nyxrobot [15], Stickybot [17], Gecko-inspired climbing robot [16], Gecko-inspired robot [20], Salamandra robotica I [12], Salamandra robotica II [13], Pleurobot [14]). IK: Inverse Kinematics.

In the section of Discussion and conclusion, we have also added:

Regarding the control mechanism (Fig. 8), most of these salamander and gecko-like robots use inverse kinematics (IK) [15], [16], [17], [20] (requiring a robot kinematic model) or/and complex multiple CPGs [12], [13], [14] (requiring a synchronization mechanism between CPGs) to generate robot gaits with C-shaped standing and/or S-shaped traveling waves. However, our simple and single CPG-based control approach neither requires a kinematic model nor a CPG synchronization to generate a trot gait with a C-shaped standing wave. In the future, we will extend our single CPG-based control with delay lines and premotor neural networks with a fast learning mechanism [31] to automatically obtain multiple gaits and various body patterns (standing and traveling waves). This extension will allow the robot to efficiently achieve different locomotion modes, such as walking, swimming, and climbing (up and down on inclined surfaces and walls). We will apply adaptive muscle models [32] to encode an elastic property resembling a real gecko-like flexible body.

[31] Thor, M., Kulvicius, T., Manoonpong P. (2020) Generic Neural Locomotion Control Framework for Legged Robots, IEEE Transactions on Neural Networks and Learning Systems, DOI: 10.1109/TNNLS.2020.3016523

[32] Huerta, C.V., Xiong, X., Billeschou, P. and Manoonpong, P., 2020, Adaptive Neuromechanical Control for Robust Behaviors of Bio-Inspired Walking Robots. In International Conference on Neural Information Processing (pp. 775-786). Springer, Cham.

Some technical word are confusing and wrong, and has to be checked. For example:- "The transfer function that determines the outputs of neurons is a hyperbolic tangent" "transfer function" in control systems is for linear systems and is based on Laplace variable, moreover it is a gain i.e. ratio between an input and an output. How can one uses the expression "transfer function" for as a signal with nonlinear hyperbolic tangent?

<u>Our answer:</u> Thank you for this comment. In fact, our transfer function here means our neural activation function that determines the outputs of neurons. To avoid the confusion, we have now corrected this as:

"**The output of the neuron is calculated using a hyperbolic tangent (tanh) activation function (i.e., $o_i = \tanh(a_i)$). Therefore, the value of o_i is between -1 and 1**."

Lateral undulation of the bendable body of a gecko-inspired robot for energy-efficient inclined surface climbing

Worasuchad Haomachai, Donghao Shao, Wei Wang, Aihong Ji, Zhendong Dai, Poramate Manoonpong*

***Abstract*—Sprawling posture animals with their bendable spine, such as salamanders, and geckos, can perform agile and versatile locomotion including walking, swimming, and climbing. Therefore, several roboticists have used them as templates for robot designs to investigate and generate efficient locomotion. Typically, walking and/or swimming abilities are realized by salamander-inspired robots with a bendable body, whereas climbing ability is achieved on gecko-inspired robots with an over-simplified fixed body. In this study, we propose optimal bendable body design with three degrees of freedom (DOFs). Its implementation on a sprawling posture robot is inspired by geckos for climbing enhancement. The robot leg and body movements are coordinated and driven by central pattern generator (CPG)-based neural control. As a consequence, the robot can climb using a combination of trot gait and lateral undulation of the bendable body with a C-shaped standing wave. Through the real robot experiments on a 3D force measuring platform, we demonstrate that, due to the dynamics of the bendable body movement, the robot can gain higher medio–lateral (F_x) ground reaction forces (GRFs) at its front legs as well as anterior–posterior (F_y) GRFs at its hind legs to increase the bending angular momentum (L_{AM}). This results in 52% and 54% reduced energy consumptions during climbing on steeper inclined solid and soft surfaces, respectively, compared to climbing with a fixed body. To this end, the study provides a basis for developing sprawling posture robots with a bendable body and neural control for energy-efficient inclined surface climbing with a possible extension towards agile and versatile locomotion, such as sprawling posture animals.**

***Keywords*—climbing robot, sprawling locomotion, bendable body, lateral undulation, central pattern generator, neural control, bending angular momentum**

I. Introduction

Sprawling animals, such as geckos and salamanders, have a bendable spine that can bend their trunk to coordinate with their limb movements during locomotion. The coordination plays a crucial role in obtaining agile locomotor capabilities (e.g., acceleration of locomotion [1] [2] [3], flexible trajectories during turning [4], stabilization of the body [5] [6], energy efficiency [7]) and versatile locomotor behaviors including walking, swimming, and climbing. Particularly, geckos not only perform various locomotion modes but also display the standing and traveling waves of lateral undulation patterns during slow-speed trotting and high-speed running, respectively. They achieve this by altering the angular velocity of the spine and limb joints, which also enhance locomotion stability [8]. Therefore, many researchers have investigated sprawling locomotion with lateral spine movement to develop robots that approach animal locomotor skills.

To date, there are two main streamlines of sprawling posture robot development. The first one focuses on the development of sprawling robots inspired by salamanders for terrestrial walking [9], [10], aquatic stepping [11], and/or swimming [12], [13], [14]. Modern sprawling robots, like Salamandra robotica [12], [13] and Pleurobot [14], can achieve not only multimodal locomotion modes but a smooth transition from swimming in water to walking on a non inclined surface and vice versa. One of key ingredients underlying the achievement is the use of a bendable segmented spine with 8-11 active joints. The spine basically improves robot locomotion through lateral undulation. The spine is designed and optimized based on the cineradiographic data from different salamander locomotion modes.

Parallel to the first streamline, the second one focuses on the development of sprawling robots inspired by geckos for terrestrial walking and/or climbing. Most gecko-inspired robots[1] mainly focus on special foot structure design [15] and the use of directional or non-directional dry adhesive materials for climbing smooth inclined and vertical surfaces [15], [16], [17], [18], [19], [20], [21]. Although they exhibit impressive climbing ability, none of them have exploited the essential role of the lateral undulation of a bendable body as realized in salamander-inspired robots and found in geckos [22] for efficient locomotion. This is because they are typically designed with an over-simplified fixed body. From this point of view, in this study we propose an optimal bendable body design with three DOFs and demonstrate its implementation on a gecko-inspired robot, Slalom (Fig. 1) for climbing enhancement on inclined surfaces. The body was designed to closely match the body lateral movement of Gekko geckos. Slalom, with its bendable body and four legs, has a total of 19 joints (i.e., three joints for the body and four for each leg), which are coordinated and driven by central pattern generator (CPG)-based neural control. The main contributions of this study include: i) a gecko-inspired bendable body design and movement for energy-efficient climbing inclined solid and soft surfaces; ii) CPG-based neural control for bendable body and leg coordination to achieve a trot gait, lateral body undulation with a C-shaped standing wave, and their combination; iii) real robot climbing experiments at different movement frequencies under different inclined angles, as well as a comparison

W. Haomachai, D. Shao, W. Wang, A. Ji, Z. Dai and P. Manoonpong are with the Institute of Bio-inspired Structure and Surface Engineering, College of Mechanical and Electrical Engineering, Nanjing University of Aeronautics and Astronautics, Nanjing, China. P. Manoonpong is also with Bio-inspired Robotics & Neural Engineering Lab, School of Information Science & Technology, Vidyasirimedhi Institute of Science & Technology, Rayong, Thailand and Embodied AI & Neurorobotics Lab, SDU Biorobotics, Mærsk Mc-Kinney Møller Institute, University of Southern Denmark, Odense, Denmark. All correspondence should be addressed to *P. Manoonpong, (poma@nuaa.edu.cn, poramate.m@vistec.ac.th)

[1]Note that, the main difference between salamander and gecko-like robots is described in the discussion section.

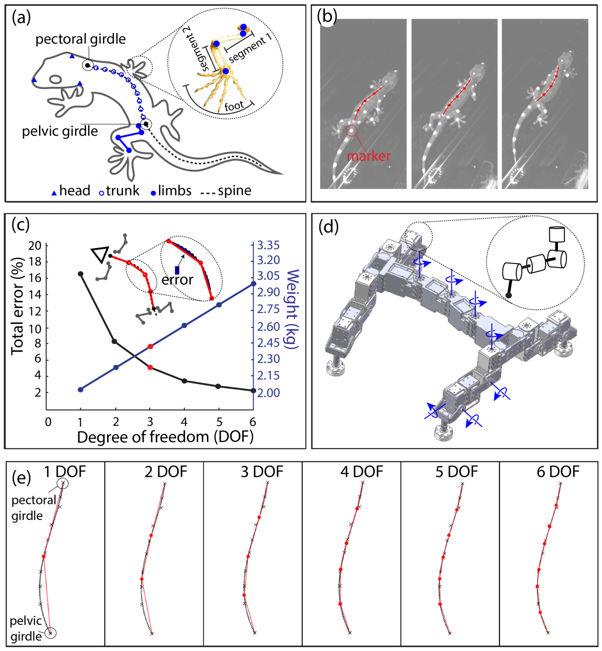

Fig. 1. The robot's spine was optimally designed to match its biological counterpart's kinematics during locomotion. We used a high-speed camera to record the Gekko gecko and the resulting three-dimensional kinematics of the skeletal structure to design the robot's body. (a) Animal morphology composed of the head, spine, and four limbs. (b) Snapshot of high-speed video of gecko movement. The white points on the gecko are reference markers for tracking the movement of its skeleton. (c) An error area between the observed trunk bending in the Gecko and the segmented line with different joint numbers were considered. The resulting number of joints (three, indicated by red point) was selected as a trade-off between the accuracy of the approximation and the minimal number of joints. Robot weight was estimated as a function of the DOFs. The robot weight was 7%, 14%, or 22% heavier than the three DOFs, when four, five, or six DOFs were selected, respectively. Likewise, the power consumption increased to 10%, 21%, 32%. (d) According to our design methodology, Slalom is constructed with a 3-DOF body and four DOFs per leg. (e) Different DOFs with symmetrical positions. Their segmented line (red line) is compared with the curvature of the gecko's body (black curve).

of climbing performance with and without the lateral body undulation, and iv) ground reaction force and bending angular momentum analysis under body movement dynamics.

II. Gecko-inspired design methodology

A. Gecko experiments and data processing

The structural design of our robot Slalom is based on the Gekko gecko which exhibits agile movement for flexible and efficient walking, running, and particularly climbing. Its morphology is composed of a head, an elongated body (trunk and tail) and four limbs located at the pectoral and pelvic girdles (Fig. 1a). The spine and leg movements during locomotion were determined from experimental videos recorded using a high-speed camera (Olympus iSpeed-3, 1280-pixel × 1024-pixel resolution, a frame rate of 500 Hz). Before each trial, the reference points were marked on the gecko's spine, head, and legs using 29 infrared reflective markers (Fig. 1b). The white circle markers were placed on the legs (12 markers), trunk (ten markers), tail (five markers), and head (two markers). The animal experiments were performed as per the Guidelines for Laboratory Animal Management in China. The experimental procedures were approved by the Jiangsu Association for Laboratory Animal Science (Jiangsu, China, approved file no. 2019-152).

The recorded videos were used to track the movement of the gecko skeleton during forward movement. For this purpose, a motion tracking software based on MATLAB (MATLAB R2019b, MathWorks, Inc.) was developed and used. The top and side views were digitized at a frame rate of 120 Hz. The body posture dataset was then used to guide an evaluation with the optimal segmentation of the robot's body (i.e., the minimum number of joints), and their placement was defined as equidistant. A comparison of the animal and robot spine structures is shown in Figs. 1a and 1d, respectively.

B. Gecko-inspired bendable body and limb design

The recorded data for the axial movements of the gecko show that during steady-state locomotion, the gecko undulated mainly in the transverse plane; bending in the sagittal plane was in a very small range [4]. This reduces the problem of designing the robot body for optimal segmentation in the transverse plane.

Each snapshot of the gecko body was represented as ten marker points in Cartesian coordinates. These points were converted to a continuous curve as the hypothetical midline of the body (body interpolation). The conversion was performed using a polynomial curve fitting function (polyfit) in MATLAB, with a fourth-degree polynomial equation. The starting point of the midline was defined as the tip of the body (the pectoral girdle) and the endpoint was defined as the end of the body (the pelvic girdle). The midline was then resampled to 100 equidistant points, which are shown by the black line in Fig. 1e. It is important to note here that the average length of all the curves in the dataset was used to define the length of the gecko's body.

To identify the best fit using the least-squares method, we performed several iterations with different numbers of joints between the defined positions of the pectoral and pelvic regions on the midline. Arbitrarily, 1-6 joints with equal distances between them were applied to different iterations (Fig. 1e). To evaluate how well the number of joints with their symmetrical positions could reproduce the curvature of the gecko's body, we introduced an error metric as the sum of the area between the segmented line and each curve in the dataset of the gecko postures (Fig. 1c).

As expected, the greater the number of joints, the better the segmented line can capture the shapes of the gecko's body during locomotion (Fig. 1c). The approximate exponential convergence of the total error value facilitated the selection of three joints, which we considered as a good trade-off based on the geometry as well as the resulting length and weight of the robot (Figs. 1c and 1d). Consequently, this optimal number with its symmetrical position allows Slalom to imitate the bending of the gecko's body in different postures during locomotion. The robot body is scaled up by increasing the size related to the ratio of the gecko's body and the size of the motors. Consequently, the final size of Slalom's body is larger than that of the gecko with a scale factor of 1:3.33.

The limbs of the gecko consist of two main segments (Fig. 1a). In our previous work [15], we described these two segments as a four-DOF limb with three DOFs at the shoulder/hip joint and one at the elbow/knee (Figs. 1d and 2c). The analysis of the kinematics suggests that all four DOFs were used during locomotion. Thus, they were all included in Slalom. Adjoining the two main segments of the limb is the foot, which has a highly complex structure with multiple compliant toes. Here, we consider the foot as a simple structure composed of two layers. The top part was built by aluminum and consists of a ball joint that provides the foot with three passive DOFs (passive wrist/ankle, Fig. 2c). This allows for the passive self-adjustment of the foot to the substrate. However, the passive movement is limited by a mechanical stopper around the ball joint. When the foot pillar reaches the stopper, it naturally changes from a freely moving part to a fixed part [15]. The range of the allowed angle movement of the pillar is ± 30 degree. The bottom layer is attached by a soft material EPDM rubber sheet for surface adhesion. Taken together, Slalom's forelimbs and hindlimbs follow the same design methodology and can perform their movements close to the gecko limb movements.

III. Slalom, a gecko-inspired robot

A. *Robot hardware setup*

Slalom has four identical limbs, each of which has four joints (Fig. 2c). The joints 1-3 correspond to the shoulder/hip joint of each front/hind leg. The joint 1 enables forward (+) and backward (-) movements, the joint 2 enables elevation (+) and depression (-) of the leg, and the joint 3 enables the attachment (-) and detachment (+) of the foot. The joint 4 corresponds to the elbow/knee joint of each front/hind leg; it enables the extension (+) and flexion (-) of the foot. The maximum and minimum ranges of the joint movements of the legs are shown in Fig. 2b. The body of Slalom consists of three joints in accordance with the optimal number of joints for the body. These body joints (BJ) can rotate around the vertical axis in a range between ± 60 degrees. It stays at zero degree during locomotion when the robot moves with a fixed body or rotates periodically when the robot moves with a bendable body. Slalom has 19 active joints in total (four at each leg, three at the body) and its weight is $2.45\,\mathrm{kg}$.

For the actuation, we chose Dynamixel XM430-W350 servomotors from ROBOTIS, Inc., as they offer an excellent trade-off featuring a fairly high torque-mass ratio (4.1 Nm of stall torque at 82g), maximum no-load speed of 46 rpm and positional accuracy (0.008 resolution) at a reasonable price. Neural control (described below) is implemented based on a robot operating system (ROS Kinetic) to control the actuators. This control system is installed on an external computer and handles the low-level communication with the servomotors through an RS-485 interface at 4 Mbps. We are able to send motor position commands and receive feedback between the servomotors at a maximum rate of 1kHz. The electrical power supply for all servomotors is provided by the adapter with a voltage regulator producing a stable 12V supply. The entire mechanical structure of Slalom is created using 3D-printing with Polylactic acid (PLA).

B. *CPG-based neural control*

This robot uses CPG-based neural control that can generate basic locomotion patterns. The entire neural control system has three components: i) a CPG mechanism with neuromodulation for generating different periodic signals and shunting inhibition for altering body joint movements, ii) neural CPG post-processing for shaping the CPG signals to obtain smooth joint movements, and iii) motor neurons for sending final motor position commands to all joints of Slalom.

The structure of this control system is based on our previous work [23] in which a chaotic CPG is modified to a simpler CPG mechanism with neuromodulation. All the neurons of the control system (Fig. 2a) are discrete-time non-spiking neurons and their update frequency is approximately 10 Hz. The activity a_i of each neuron develops according to the following equation:

$$a_i(t) = \sum_{j=1}^{n} W_{ij} \cdot o_j(t-1) + B_i, \quad i = 1, ..., n., \qquad (1)$$

where n denotes the number of neurons, B_i an internal bias term along with a stationary input to neuron i, and W_{ij} the synaptic strength of the connection from neuron j to neuron i. The output of the neuron is calculated using a hyperbolic tangent ($tanh$) activation function (i.e., $o_i = tanh(a_i)$). Therefore, the value of o_i is between -1 and 1.

The CPG is a recurrent neural network with two fully connected neurons (Fig. 2a). This main network generates periodic signals for locomotion. Recurrent weights between both neurons are determined by $W_{12} = 0.18 + MI, W_{21} = -W_{12}$, whereas weights $W_{11,22}$ are set to 1.4. MI is an extrinsic modulatory input used to generate different stride frequencies of moving gait. This parameter setup with $MI = 0.08$ results in the lowest stride frequency of $0.10\,\mathrm{Hz}$. Increasing MI will increase the stride frequency of moving (Fig. 3a). However, MI is limited at 0.26 (stride frequency of $0.25\,\mathrm{Hz}$) because the motor of Slalom cannot properly follow the high driving frequency. The investigation of Slalom climbing on inclined surfaces using this CPG shows that its moving speed is proportional to the value of MI; i.e., increasing MI leads to an increase in fast moving speed (Fig. 3d). In addition, Slalom uses the same gait (trot gait) at different values of MI in our study.

The outputs of the CPG (c_i) are passed to the motor neurons through both shunting inhibition and CPG postprocessing (Fig. 2a). The shunting inhibition neuron (SI) is inspired by neurophysiological findings [24]. The neuron receives one inhibitory input (I) and one excitatory input from the CPG neuron 1 (c_1). We manually control the inhibitory input by setting it to either 0 (inactive) or 1 (active) (i.e., $I = 1$ results in the shunting inhibition neuron being inhibited) and the SI is stimulated by receiving the excitatory input. When the inhibitory and excitatory inputs are stimulated simultaneously, the output of the CPG leaks out before it reaches the motor neurons. However, when the inhibitory input is not stimulated ($I = 0$), the output of the CPG is directly sent to the motor neurons (body joints, $BJ_{1,2,3}$). It indicates that the robot moves with a bendable body when I is set to 0 while $I = 1$ is

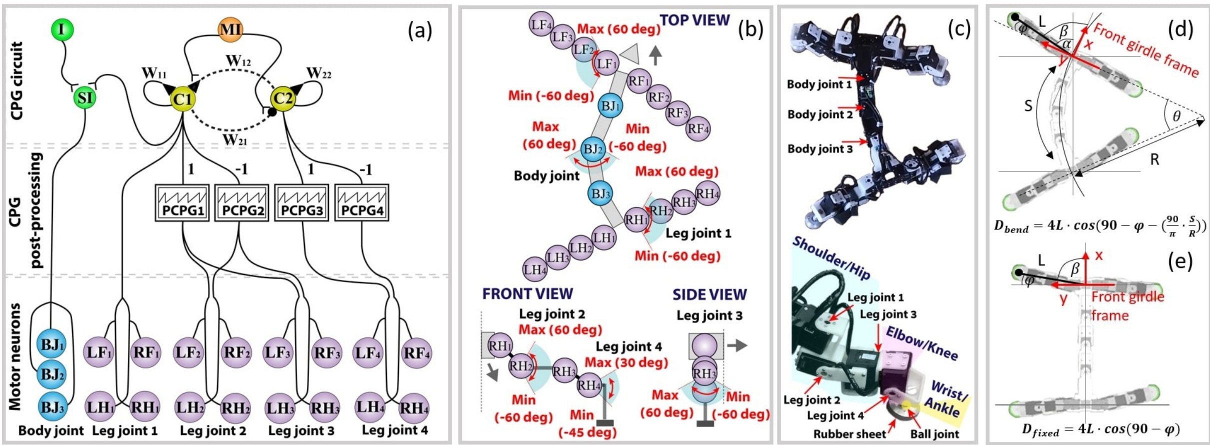

Fig. 2. Architecture of the simplified CPG-based controller. (a) Neural circuit for controlling the gecko-inspired robot. (b) Location of the motor neurons on the robot and their movements. Minimum and maximum angles of the body joints, leg joint 1, leg joint 2, leg joint 3 and leg joint 4. (c) Example of components at the body joints and the left hind leg (LH). (d), (e) Geometrical models of the bendable and fixed bodies. The models can be used to analyze the energy efficiency improvement based on a stride length of the bendable robot body (D_{bend}) compared with the fixed robot body (D_{fixed}). φ is the angle between the foot location and the y-axis of the girdle frame at the beginning of each stride (i.e., 17 degrees). R is the bending radius of the bendable body (i.e., 41.7 cm). L is the leg length (i.e., 17.3 cm). S is the body length (i.e., 35 cm). According to the parameter values obtained from the real robot movements driven by the neural control, D_{bend} is approximately 2.24 times larger than D_{fixed}. The bendable-body robot treaded longer than the fixed-body robot during each stride. Therefore, the cost of transport (COT) of the bendable-body robot was lower than that of the fixed-body robot (COT$_{bend} \cong \frac{COT_{fixed}}{2.24}$, assuming that both robot configurations have the same mess (m) and almost the same energy usage (E)). The COT formula is shown in section IV. D_{bend} and D_{fixed} derivation formulae can be accessed at https://bit.ly/3fXxLjH. Our robot climbing experimental observations (Fig. 5) followed COT estimations.

for a fixed body. The model of the shunting inhibition neural unit is described by:

$$SI(t) = (1 - I) \cdot c_1(t). \tag{2}$$

The CPG post-processing (PCPG) units receive two different input signals consisting of the original and inverse of the CPG output. For instance, the first PCPG unit ($PCPG_1$) directly receives the CPG output while the second PCPG unit ($PCPG_2$) is given by a multiplication of -1 and the output of CPG (inverted CPG output). The post-processing units shape the CPG signals to the asymmetry of ascending and descending slopes (Fig. 3c) as follows. First, the input signals are transformed by the units which produce the step function outputs (Equation 3) with high (1) or low (0) values. Second, the high and low outputs are converted into continuous signals with exponentially ascending and dramatically descending slopes, respectively. The conversion is done as follows:

$$f(c_i(t)) = \begin{cases} 1, & \text{if } -0.87 < c_i(t) < 0.87 \quad \text{and} \quad \frac{\partial c_i(t)}{\partial t} > 0, \\ 0, & \text{otherwise,} \end{cases} \tag{3}$$

$$PCPG_n = f(c_i(t)) \cdot [-1^{(n+1)} \cdot c_i(t)], \tag{4}$$

where n denotes the number of PCPG units and c_i is the outputs of CPG neuron i. According to this, the post-processing CPG outputs are scaled to the range between -1.0 and 1.0. It should be noted that different frequencies of the CPG generate different ascending slopes (Fig. 3c).

The outputs of the post-processing CPG units are directly sent to the motor neurons of the leg joint 2, 3, and 4. The shunting inhibition and CPG outputs are directly sent to the motor neurons of the body joints and leg joint 1, respectively (Fig. 2a). The diagonal joints receive an identical signal, whereas the other diagonal joints receive a 90° phase-shifted signal. This setup leads to biologically inspired leg coordination since the legs on each side perform phase-shifted movements of the same frequency [25]. The frequency of the signals is defined by MI of the CPG. Figure 3d illustrates four leg movements during moving forward from low to high frequencies. Slalom shows a trot gait in which the swing and stance phases of the diagonal legs occur simultaneously. The C++ code of the CPG-based control can be accessed from https://bit.ly/3fXxLjH.

IV. Experimental validation of Slalom

To verify the locomotor abilities of our robot in this design, we carried out a series of experiments that compared the locomotion of the robot with the lateral undulation of the body (bendable body) and the absence of lateral body movement (fixed body). We used the cost of transport (COT), robot speed, and slope angle for our validation. In addition, the ground reaction force and bending angular momentum were analyzed to verify the effect of the bendable body on the ability to climb an inclined surface.

A. Experimental set-up for robot experiments

In this study, the robot was built based on the Gekko gecko and tested in the real environment. Five main experiments were conducted for different stride frequencies of $0.10, 0.15, 0.19, 0.22, 0.25$ Hz to study the robot performance when climbing different slope angles ($0, 15, 20, 25, 30$ degrees). The fastest stride frequency was limited to $0.25\,\text{Hz}$ owing to hardware limitations. The experimental data was recorded for 10 trials while traversing a 1 m distance. We structured the slope into two layers: the top layer employed

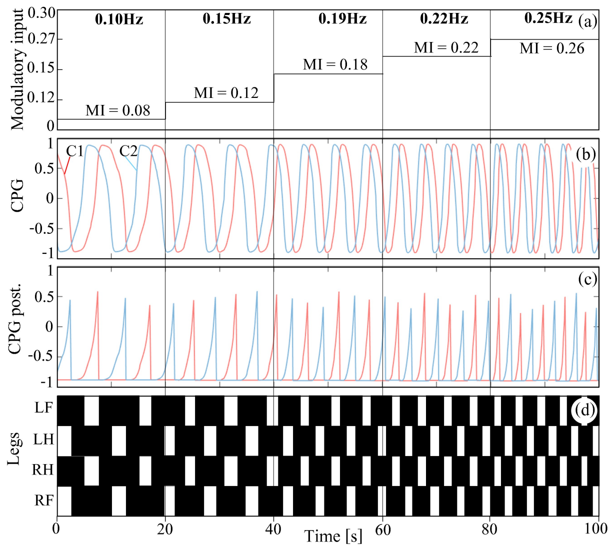

Fig. 3. Examples of trot gait generated by the neural control at five different stride frequencies. (a) Increasing the CPG output frequency trough MI. (b) The CPG output signals. (c) The CPG post-processing output signals. (d) Gait diagram. The black and white areas indicate the stance and swing phases, respectively.

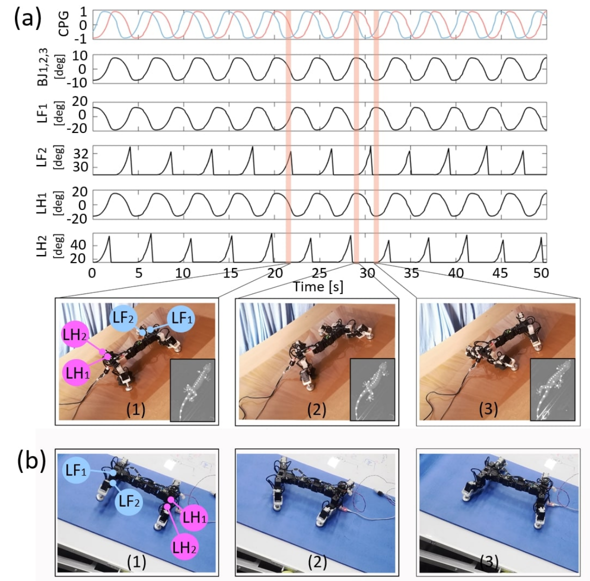

Fig. 4. Example of Slalom locomotion with the bendable body on solid and soft inclined surfaces. (a) The top graph shows the CPG output signals. The other graphs show the joint angles of the body ($BJ_{1,2,3}$, see Fig. 2b), left front ($LF_{1,2}$, see Fig. 2b), and left hind ($LH_{1,2}$, see Fig. 2b). The snapshots below illustrate the postures of the robot and gecko during climbing on an inclined solid surface. (b) The snapshots depict the robotic postures while climbing a soft inclined surface. A video of the experiments can be seen at http://www.manoonpong.com/Slalom/Video1.mp4.

either an acrylic sheet or a foam mat (stiffness of 5 N/mm) as solid or soft climbing surface, respectively and the bottom layer was built with plywood for structural support. The dimension of the slope was 1 m $\times$ 1.5 m.

COT was calculated using the equation COT = E/mgd [26]. E denotes the energy consumed during locomotion, which was calculated using the servo motor embedded sensors. These sensors measured the power consumed by the 19 Slalom servo motors. m, g, and d denote the robot mass (2.45 kg), acceleration due to gravity (9.81 m/s^2), and displacement (1 m), respectively.

B. Robot climbing experiments

This climbing experiments evaluated energy efficiency while moving forward at different solid and soft inclined surfaces with bendable and fixed-body modes. During locomotion, the CPG-based control generated the trot gait. For the bendable body, the gait involves the body oscillation with a C-shaped standing wave that is well-coordinated with the limbs. On solid slopes, different speeds ($0.10, 0.15, 0.19, 0.22,$ and 0.25 Hz) were investigated, whereas on soft slopes, only the most energy-efficient climbing speed (0.25 Hz) realized from solid slope climbing was investigated.

Figure 4a shows an example of the CPG-based control signals during climbing with the bendable body and a stride frequency of 0.25 Hz on the 15-degree solid slope. It should be noted that the signals of the diagonal legs are identical. For instance, the signal of the left front joint 1 (LF_1) is equal to that of the right hind joint 1 (RH_1), and the right front joint 2 (RF_2) and the left hind joint 2 (LH_2) also have the same signal. Furthermore, in each local leg, the signals of both joints 3 and 4 are similar to that of joint 2 but with different amplitudes. Such control strategies were applied while climbing on soft slopes. Snapshots of Fig. 4a depict a 15-degree climbing by the robot on a solid inclined surface, which corresponds to the red areas of the control signals. Photo 1 illustrates the swing phase in which the body joints reached the middle position while rotating from the right side to the left; the elevation of LF_2 and RH_2 was observed, while RF_2 and LH_2 stayed on the ground. Photo 2 shows the stance phase in which the body flexion appeared as a C-shaped standing wave on the right side while all the limbs stayed on the ground. Photo 3 shows the robot performing the opposite C-shaped body flexion during the stance phase. Similar climbing behavior was observed on a 15-degree soft inclined surface (Fig. 4b).

The results of climbing experiments (Fig. 5), show that the COT tends to decrease when the frequency is increased for each solid slope angle. For instance, for the fixed body at a slope with 25 degrees, the robot consumes a COT of approximately 172 at 0.10 Hz, and then begins a sharp downward trend to approximately $137, 109, 94,$ and 84 when the frequency is increased to $0.15, 0.19, 0.22,$ and 0.25 Hz, respectively. The COT also tends to a similar direction to that the bendable body. It is clear that this solid-slope climbing experiment provided a stride frequency of 0.25 Hz, which consumed the lowest COT on each slope, and consequently it was defined as the optimal moving speed. This frequency was employed in the soft inclined surface climbing experiment (Fig. 5). While the bendable-body robot climbed solid and soft surfaces inclined up to 30 and 25 degrees, respectively, the fixed-body robot climbed those inclined up to 25 and 20 degrees, respectively.

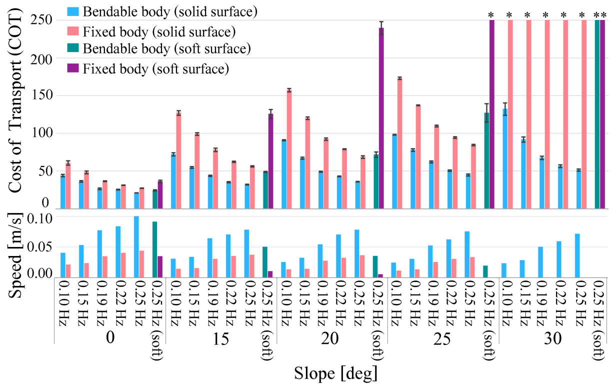

Fig. 5. (a) COT and (b) climbing speed are being compared between movements with bendable and fixed body modes on various solid and soft slopes (0, 15, 20, 25, and 30 degree). "*" indicates the cases in which the robot failed to climb the inclined surfaces and resulted in a COT > 250.

C. Ground reaction force analysis

To explain why Slalom archived a higher slope angle when it coordinates periodic lateral body flexion and limb movements during climbing. We investigated the interaction forces between the robot and the environment, and quantified them by comparing the GRFs between the robot with and without the bendable body. The results of the GRF analysis are presented in Fig. 6; when Slalom moves with a lateral undulation of the bendable body, the lateral peak force (F_x) was -2 N (see (a) in Fig. 6), and the forelimb of robot is pushed outward from the body. The force gradually increases until it reaches the medio peak force (F_x) of 4 N (see (b) in Fig. 6), suggesting that Slalom pulled its forelimb inward toward the body. Although the forelimb slips (see (c) in Fig. 6) in the case with the bendable body, it can quickly recover to a normal stance. This indicates that the forelimbs make a significant effort to prevent the robot's head from moving sideways in the second half of the stance phase. Typically, a larger medio force provides higher protection of the Slalom's head tilting out in order to maintain the movement while stepping forward. In this case, the bendable-body robot exhibited larger medio force than the fixed-body robot (see (b) in Fig. 6).

Furthermore, the GRFs illustrate that most of the propulsion in the robot is generated by its hindlimbs, as indicated by the posterior forces (F_y). More specifically, the robot with the bendable body has shown the posterior peak force of 6 N (see (e) in Fig. 6) for the hindlimbs while the forelimbs always produce a force below 4 N (see (d) in Fig. 6). Moreover, the climbing experiments with the bendable body produced approximately 3 N larger posterior forces in the hindlimbs (left hindlimb) than that with the fixed body during $45\% - 65\%$ of the stance phase (see (e) in Fig. 6). Normally, the limbs generate a positive posterior force when the robot propels itself forward by pushing the limbs backward. It is evident that the larger the value of posterior force, the higher the angle of slope the robot can climb.

Finally, we observed similar characteristics in the normal forces (F_z) for both the bendable and fixed bodies, where the normal forces peaked from 35% to 65% (see (f) in Fig. 6) during the stance phase for both the hindlimbs and forelimbs: however, larger fluctuations in force amplitude were observed with the bendable body. This indicates that the diagonal limbs have to bear most of the load in the middle of the stance phase.

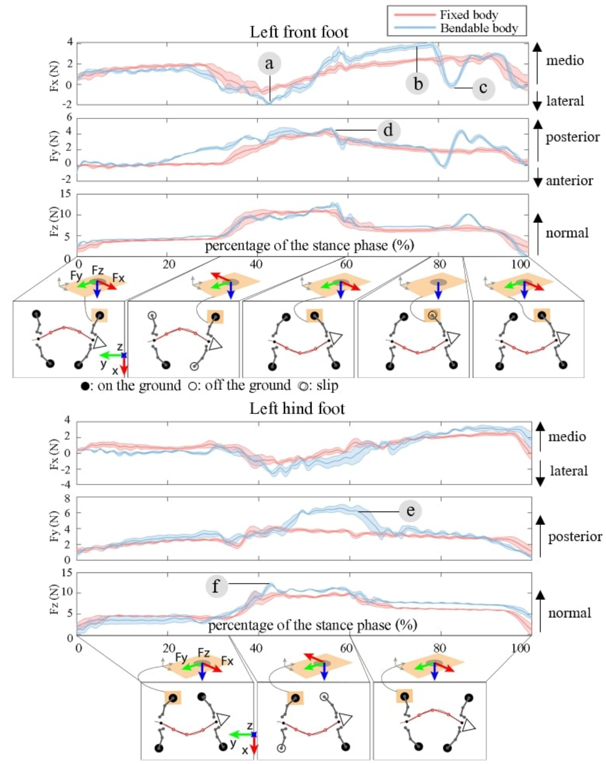

Fig. 6. Comparison of ground reaction forces (GRFs) in fixed and bendable body movements. Left forelimb and left hindlimb GRFs were measured and analysed with respect to medio-lateral (F_x), anterior-posterior (F_y) and normal (F_z). The robot with the bendable body produces medio-lateral forces in the forelimb, including (a) lateral peak force, (b) medio peak force, and (c) lateral force during slip. For anterior-posterior forces, the forelimb always produces a posterior force below 4 N (d) while the force reaches 6 N (e) for the hindlimb. The normal forces of both the bendable and fixed bodies are similar (f). Each snapshot below show the body postures and the position of feet on/off the ground during climbing.

D. Bending angular momentum

Based on the robot's movement dynamics caused by the continuous action of the ground reaction force, we introduce the bending angular momentum (L_{AM}) to reveal the contribution of the forelimb, hindlimb and body for maintaining the robot's movement. Mathematically, L_{AM} is defined as Equation (5) using the center of mass (COM) of the robot as the center of the bending moment.

$$L_{AM} = \left| \int_0^{T_s} -\vec{c} \times \vec{F}_{HP} \mathrm{d}t + \int_0^{T_s} -\vec{d} \times \vec{F}_{HL} \mathrm{d}t + \int_0^{T_s} (\vec{a} - \vec{c}) \times \vec{F}_{FP} \mathrm{d}t + \int_0^{T_s} (\vec{b} - \vec{d}) \times \vec{F}_{FL} \mathrm{d}t \right|, \tag{5}$$

where T_s is the duration of the stance phase, the medio-lateral and anterior-posterior forces are produced by the hind foot (F_{HL} and F_{HP}) and the front foot (F_{FL} and F_{FP}). The medio-lateral (a) and anterior-posterior (b) distances between the left and right support feet, the medio-lateral (c) and anterior-posterior (d) distances between the COM and the hind support feet are demonstrated with by similar diagrams of animals and robots in Figs. 7a and 7b, respectively. Generally,

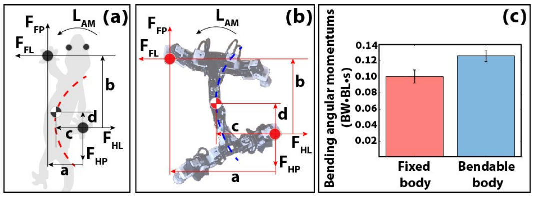

Fig. 7. A bending angular momentums is induced by GRFs during a step. (a) Gecko and (b) robot diagram of the calculation for bending angular momentum, where the center of mass was used as the center of the bending moment to calculate the bending angular momentum generated by the feet. (c) Comparison between the mean values of the bending angular momentum during robot climbing with fixed and bendable bodies. BW: body weight; BL: body length.

a greater amount of L_{AM} results in higher climbing stability on an inclined slope. The stability is obtained because of the large medio and posterior forces, which cause the COM to oscillate laterally from side to side while a pair of diagonal supporting limbs contacts the ground intermittently in a stride. The center of the bending moment (Fig. 7b) demonstrates the COM dynamics, which is explained by applying the lateral leg spring (LLS) model [27]. Perturbation experiments illustrated that the sprawling posture animal LLS models self-stabilized, despite control feedback [28]. The model was stable as the medio-lateral and anterior-posterior forces produced the lateral angular momentum that incurred in leg-to-leg transitions [29].

We converted the bending angular momentum into body weight-body length-seconds (BW·BL·s) and compared the results between the robot's moment with and without the bendable body (Fig. 7c). The mean values of L_{AM} of robot climbing with the bendable body is 0.125, which is approximately 25% higher than that of the fixed body. This indicates that the lateral undulation of the bendable body during climbing contributes not only to a transition of forces between the forelimbs and hindlimbs, but also to maintaining stability for continuity of the locomotion due to the gains of bending angular momentum. It is evident that the bendable body is used to archive the ability to climb surfaces with higher inclinations, similar to the case of geckos when climbing up slopes. To maintain their movement, they bend the spine to increase the bending angular momentum when the slope increases [30].

V. Discussion and Conclusion

We presented a systematic way to design the bendable body of a gecko-inspired robot, which is based on an experiment involving a high-speed camera recording of the movement of a Gekko gecko. The body movements of a gecko were analyzed to determine the optimal number of body joints. We used a bio-inspired approach to construct Slalom, a gecko-like robot with three body joints and four joints at each leg (19 DOFs in total) to emulate the sequence of gecko postures. CPG-based neural control with a neuromodulation (MI) was introduced to control the moving gait of Slalom. This control model is directly inspired by the biological findings and is well suited for generating a trot gait at different frequencies.

This study also demonstrated the climbing abilities of a gecko-inspired robot with lateral undulation of the bendable body. We performed a series of climbing experiments to evaluate the robot performance with and without the bendable body. The results show that the optimal locomotion speed of Slalom is at the highest stride frequency (0.25 Hz).

Moreover, it was shown that there are two reasons why a bendable body is advantageous compared to a fixed body in term of energy efficiency and efficient climbing. First, the COT of the bendable body was approximately 52% (54%) lower than that of the fixed body for all solid (soft) slopes when the robot moved at the same stride frequency (Fig. 5). Second, Slalom with the bendable body can climb a steeper slope (Fig. 5). For instance, it was unable to climb with the fixed body at a 30-degree solid slope and a 25-degree soft slope. This is because, when the angles of the solid and soft slopes were greater than 25 and 20 degrees, respectively, it began to slip on the solid slope and to get stuck on the soft slope (see http://www.manoonpong.com/Slalom/Video1.mp4).

GRF analysis demonstrated that the robot's hindlimbs generated most of the propulsion, as indicated by the posterior forces. The medio forces indicated that the forelimbs prevented the robot's head from moving sideways. The bendable-body robot exhibited greater hindlimb posterior force and forelimb medio force than the fixed-body robot. This enhanced the robot's stability while climbing steeper slopes. We calculated the bending angular momentum that resulted from the forces acting on the feet. The bendable-body robot produced a larger angular momentum, which was essential for stability during climbing. Here, the robot produced almost similar L_{AM} for all the inclined slopes where the bending radius of the bendable body was constant. In the future, we will investigate the change of bending radius to increase L_{AM} when encountering an increased slope angle, as observed in geckos [30].

Compared to existing salamander and gecko-like robots [12], [13], [14], [15], [16], [17], [20] (Fig. 8), the existing robots were designed with different structure in order to approach animal locomotor skills. Salamander robots were developed with a bendable body and leg structure with simple point-contact elements of the foot, while most of the gecko robots were constructed with an oversimplified fixed body and a complex leg structure with a special foot design with an adhesive material. In this study, Slalom has a bendable body like most salamander robots and a complex gecko-based leg structure with four DOFs and a flat foot with a passive ankle at each leg. This ankle and foot design will allow us to later implement a bio-inspired dry adhesive material with a mushroom-shaped microstructure, like other gecko robots, for energy-efficient climbing of highly inclined slopes and walls. In principle, our robot design bridges the gap between the salamander and gecko-like robots.

Regarding control mechanisms (Fig. 8), most of these salamander and gecko-like robots use inverse kinematics (IK) [15], [16], [17], [20] (requiring a robot kinematic model) or/and complex multiple CPGs [12], [13], [14] (requiring a synchronization mechanism between CPGs) to generate robot gaits with C-shaped standing and/or S-shaped traveling waves. However, our simple and single CPG-based control approach neither requires a kinematic model nor a CPG synchronization to generate a trot gait with a C-shaped standing wave. In

Robot	Control method	Multi-segmented body	Limb structure (can use adhesive material)	Locomotion modes			Surface		
				Horizontal	Slope	Vertical	Solid	Soft	Liquid
Our robot (Slalom)	CPG	✓	✓	✓	✓	✗	✓	✓	✗
Nyxrobot	IK	✗	✓	✓	✓	✗	✓	✗	✗
Stickybot	IK, Force-based controller	✗	✓	✗	✗	✓	✓	✗	✗
Gecko-inspired climbing robot	IK, Open loop controller	✗	✓	✗	✗	✓	✓	✗	✗
Gecko-inspired robot	IK, Open loop controller	✗	✓	✗	✗	✓	✓	✗	✗
Salamandra robotica I	CPGs	✓	✗	✓	✗	✗	✓	✗	✓
Salamandra robotica II	CPGs	✓	✗	✓	✗	✗	✓	✗	✓
Pleurobot	CPGs, IK	✓	✗	✓	✗	✗	✓	✗	✓

Fig. 8. A comparison between our robot (Slalom) and the other state-of-the-art sprawling posture robots (Nyxrobot [15], Stickybot [17], Gecko-inspired climbing robot [16], Gecko-inspired robot [20], Salamandra robotica I [12], Salamandra robotica II [13], Pleurobot [14]). IK: Inverse kinematics.

the future, we will extend our single CPG-based control with delay lines and premotor neural networks with a fast learning mechanism [31] to automatically obtain multiple gaits and various body patterns (standing and traveling waves). This extension will allow the robot to efficiently achieve different locomotion modes, such as walking, swimming, and climbing (up and down on inclined surfaces and walls). We will apply adaptive muscle models [32] to encode an elastic property resembling a real gecko-like flexible body.

VI. Acknowledgment

We thank Stanislav Gorb for fruitful discussions, Pongsiri Borijindakul for experimental support, and Sun Tao for comments. This work was supported by NSFC (Grant No. 51861135306) [PM, AJ] and the National Key R&D Program of China (2020YFB1313504)[PM].

References

[1] A. Zaaf, R. Van Damme, A. Herrel, and P. Aerts, "Spatio-temporal gait characteristics of level and vertical locomotion in a ground-dwelling and a climbing gecko," *Journal of Experimental Biology*, 2001.

[2] K. Karakasiliotis and A. J. Ijspeert, "Analysis of the terrestrial locomotion of a salamander robot," in *2009 IEEE/RSJ International Conference on Intelligent Robots and Systems*, Oct. 2009, pages 5015–5020.

[3] W. Nam, T. Seo, B. Kim, D. Jeon, K.-J. Cho, and J. Kim, "Kinematic analysis and experimental verification on the locomotion of gecko," *Journal of Bionic Engineering*, pages 246–254, 2009.

[4] K. Autumn, S. T. Hsieh, D. M. Dudek, J. Chen, C. Chitaphan, and R. J. Full, "Dynamics of geckos running vertically," *Journal of Experimental Biology*, volume 209, number 2, pages 260–272, 2006.

[5] J. J. Chen, A. M. Peattie, K. Autumn, and R. J. Full, "Differential leg function in a sprawled-posture quadrupedal trotter," *Journal of Experimental Biology*, volume 209, number 2, pages 249–259, 2006.

[6] D. I. Goldman, T. S. Chen, D. M. Dudek, and R. J. Full, "Dynamics of rapid vertical climbing in cockroaches reveals a template.," eng, *J Exp Biol*, volume 209, number Pt 15, pages 2990–3000, Aug. 2006.

[7] W. Wang, S. Wu, P. Zhu, and R. Liu, "Analysis on the dynamic climbing forces of a gecko inspired climbing robot based on gpl model," in *2015 IEEE/RSJ International Conference on Intelligent Robots and Systems (IROS)*, Sep. 2015, pages 3314–3319.

[8] W. Wang, A. Ji, Z. Dai, G. Qin, X. zhang, T. Ren, and Q. Han, "Angular variables of climbing geckos in two lateral undulation patterns," *Zoology*, page 125 892, 2020.

[9] R. Breithaupt, J. Dahnke, K. Zahedi, J. Hertzberg, and F. Pasemann, "Robo-salamander - an approach for the benefit of both robotics and biology," 2002.

[10] B. Chong, Y. Aydin, C. Gong, G. Sartoretti, Y. Wu, J. Rieser, H. Xing, J. W. Rankin, K. Michel, A. G. Nicieza, J. Hutchinson, D. Goldman, and H. Choset, "Coordination of back bending and leg movements for quadrupedal locomotion," in *Robotics: Science and Systems*, 2018.

[11] A. A. M. Faudzi, M. R. M. Razif, G. Endo, H. Nabae, and K. Suzumori, "Soft-amphibious robot using thin and soft mckibben actuator," in *2017 IEEE International Conference on Advanced Intelligent Mechatronics (AIM)*, 2017, pages 981–986.

[12] A. J. Ijspeert, A. Crespi, D. Ryczko, and J.-M. Cabelguen, "From swimming to walking with a salamander robot driven by a spinal cord model," *Science*, volume 315, number 5817, pages 1416–1420, 2007.

[13] A. Crespi, K. Karakasiliotis, A. Guignard, and A. J. Ijspeert, "Salamandra robotica ii: An amphibious robot to study salamander-like swimming and walking gaits," *IEEE Transactions on Robotics*, volume 29, number 2, pages 308–320, 2013.

[14] K. Karakasiliotis, R. Thandiackal, K. Melo, T. Horvat, N. K. Mahabadi, S. Tsitkov, J. M. Cabelguen, and A. J. Ijspeert, "From cineradiography to biorobots: An approach for designing robots to emulate and study animal locomotion," *Journal of The Royal Society Interface*, volume 13, number 119, page 20 151 089, 2016.

[15] D. Shao, J. Chen, A. Ji, Z. Dai, and P. Manoonpong, "Hybrid soft-rigid foot with dry adhesive material designed for a gecko-inspired climbing robot," in *2020 3rd IEEE International Conference on Soft Robotics (RoboSoft)*, 2020, pages 578–585.

[16] A. Ji, Z. Zhao, P. Manoonpong, W. Wang, G. Chen, and Z. Dai, "A bio-inspired climbing robot with flexible pads and claws," *Journal of Bionic Engineering*, volume 15, number 2, pages 368–378, 2018.

[17] S. Kim, M. Spenko, S. Trujillo, B. Heyneman, D. Santos, and M. Cutkosky, "Smooth vertical surface climbing with directional adhesion," *IEEE Transactions on Robotics*, volume 24, pages 65–74, 2008.

[18] O. Unver and M. Sitti, "A miniature ceiling walking robot with flat tacky elastomeric footpads," in *2009 IEEE International Conference on Robotics and Automation*, 2009, pages 2276–2281.

[19] Y. Liu, H. Kim, and T. Seo, "Anyclimb: A new wall-climbing robotic platform for various curvatures," *IEEE/ASME Transactions on Mechatronics*, volume 21, number 4, pages 1812–1821, 2016.

[20] M. P. Murphy, C. Kute, Y. Mengüç, and M. Sitti, "Waalbot ii: Adhesion recovery and improved performance of a climbing robot using fibrillar adhesives," *The International Journal of Robotics Research*, volume 30, number 1, pages 118–133, 2011.

[21] Z. Wang, Z. Wang, Z. Dai, and S. Gorb, "Bio-inspired adhesive footpad for legged robot climbing under reduced gravity: Multiple toes facilitate stable attachment," *Applied Sciences*, page 114, 2018.

[22] W. Wang, A. Ji, P. Manoonpong, H. Shen, J. Hu, Z. Dai, and Z. Yu, "Lateral undulation of the flexible spine of sprawling posture vertebrates," *Journal of Comparative Physiology A*, volume 204, number 8, pages 707–719, Jul. 2018.

[23] P. Manoonpong, U. Parlitz, and F. Wörgötter, "Neural control and adaptive neural forward models for insect-like, energy-efficient, and adaptable locomotion of walking machines," *Frontiers in Neural Circuits*, volume 7, page 12, 2013.

[24] W. Paulus and J. C. Rothwell, "Membrane resistance and shunting inhibition: Where biophysics meets state-dependent human neurophysiology.," eng, *J Physiol*, pages 2719–2728, 2016.

[25] D. M. Wilson, "Insect walking," *Annual Review of Entomology*, volume 11, number 1, pages 103–122, 1966.

[26] K. Mombaur, H. Vallery, Y. Hu, J. Buchli, P. Bhounsule, T. Boaventura, P. M. Wensing, S. Revzen, A. D. Ames, I. Poulakakis, and A. Ijspeert, "Chapter 4 - control of motion and compliance," in *Bioinspired Legged Locomotion*, Butterworth-Heinemann, 2017, pages 135–346.

[27] J. Schmitt and P. Holmes, "Mechanical models for insect locomotion: Dynamics and stability in the horizontal plane i. theory," *Biological Cybernetics*, volume 83, number 6, pages 501–515, 2000.

[28] T. M. Kubow, "The role of the mechanical system in control: A hypothesis of self-stabilization in hexapedal runners," *Philosophical Transactions of the Royal Society B: Biological Sciences*, volume 354, number 1385, pages 849–861, May 1999.

[29] J. Schmitt, M. Garcia, R. C. Razo, P. Holmes, and R. J. Full, "Dynamics and stability of legged locomotion in the horizontal plane: A test case using insects," *Biological Cybernetics*, volume 86, number 5, pages 343–353, 2002.

[30] Z. Wang, L. Cai, W. Li, A. Ji, W. Wang, and Z. Dai, "Effect of slope degree on the lateral bending in gekko geckos," *Journal of Bionic Engineering*, volume 12, number 2, pages 238–249, 2015.

[31] M. Thor, T. Kulvicius, and P. Manoonpong, "Generic neural locomotion control framework for legged robots," *IEEE Transactions on Neural Networks and Learning Systems*, pages 1–13, 2020.

[32] C. V. Huerta, X. Xiong, P. Billeschou, and P. Manoonpong, "Adaptive neuromechanical control for robust behaviors of bio-inspired walking robots," in *Neural Information Processing*, Cham: Springer International Publishing, 2020, pages 775–786.